Echinoderm stabilization associated with a paleokarst surface at the Mississippian-Pennsylvanian boundary in Tennessee

KENNETH J. TOBIN[1], and STEVEN G. DRIESE[2]

[1] Department of Natural Sciences; Texas A&M International University; 5201 University Blvd.; Laredo, TX, 78041

[2] Department of Geological Sciences; University of Tennessee-Knoxville; Knoxville, TN 37996-1410

manuscript received_____; revised_____

Version: January 18, 2002

Running title: *Paleokarst and Calcite Diagenesis*

Keyword: Paleokarst, Paleosols, Calcite Diagenesis, Iron Reduction, Quantitative Modeling

ABSTRACT

Pennington Formation limestone deposits in Tennessee have echinoderm grains that exhibit spatial variations in minor element and stable isotopic compositions with respect to the paleokarst surface that defines the Mississippian-Pennsylvanian stratigraphic contact. Echinoderm grains immediately below the paleokarst surface have lower Mg and $\delta^{13}C$ values with higher Fe concentrations compared with grains meters below the paleokarst surface. Additionally, covariation of $\delta^{13}C$ and $\delta^{18}O$ values recorded from echinoderm grains is indicative of alteration of these allochems under meteoric conditions. Paleosols draping the paleokarst surface and coal seams, which were deposited immediately above the Mississippian-Pennsylvanian contact, provided ample organic matter that could have driven heterotrophic microbial activity. Additionally, the paleosols were an ample source of oxidized Fe that could have used as a terminal electron acceptor by an anaerobic microbial community. Therefore, we suggest that microbial iron reduction transferred Fe from the paleosol to meteoric diagenetic calcite during meteoric stabilization of echinoderm grains, which is supported by quantitative modeling of carbonate solubility (PHREEQC) and iterative modeling of diagenetic calcite minor element and stable isotopic compositions.

INTRODUCTION

The purpose of this paper is to constrain the geochemical conditions associated with echinoderm stabilization from the Pennington Formation (Late Mississippian). This paper is unique in its combination of two approaches that are used to constrain diagenetic fluid composition. Mineral saturation indexes using the computer program PHREEQC (Parkhurst and Appelo 1999) determine whether modeled solution is undersaturated with respect to calcite; a necessary condition for echinoderm stabilization to proceed. Additionally, iterative modeling (Banner and Hanson 1990) is used to constrain calcite minor element and stable isotopic compositions. Convergence of calculated cumulative fluid-rock values (N) from iterative modeling that are necessary to obtain observed echinoderm calcite Mg, Fe, $\delta^{13}C$, and $\delta^{18}O$ values

provides an additional constrain on diagenetic fluid composition. Significantly, these approaches can be applied to the modeling of any diagenetic system consisting of metastable carbonate phases undergoing stabilization.

Additionally, this study elucidates an aspect of the iron cycle documenting the linkage between oxidized Fe in paleosol and reduced Fe in stabilized echinoderm grains present in subjacent limestone deposits. This paper documents spatial trends in carbonate geochemistry over an interval of only a few meters. In modern meteoric systems, steep gradients in the redox chemistry of natural water can occur over the meter scale (*e.g.* Bjerg et al. 1995;) and the connection between the chemistry of redox sensitive elements and *in situ* microbial activity, such as Fe reduction, is becoming apparent (e.g., McMahon and Chapelle 1991; Murphy and Schramke 1998). In pristine natural systems steep spatial gradients in microbial terminal electron acceptor utilization have been linked with lithologic discontinuities (Fredrickson et al. 1997). However, establishing the microbial-geochemical correlation in ancient carbonate systems is much more equivocal. While abiotic redox cycling of Fe between paleosol and subjacent Pennington limestone is possible given the ubiquitous nature of microorganisms in shallow subsurface settings (Parkes et al. 1994) microbial Fe reduction is a more plausible mechanism for transferring Fe from paleosol to calcite. This paper is an addition contribution to the literature that indirectly infers microbial activity in ancient carbonate sequences (*e.g*. Hendry 1993; Tobin et al. 1996).

GEOLOGICAL SETTING

The Pennington Formation is of latest Chesterian age (Crawford 1985; Patchen et al. 1985) and ranges from 30-150 m in thickness. It is a mixed siliciclastic-carbonate succession that consists of interstratified dolostone, limestone, variegated shale (that ranges from red to greenish-gray and includes many paleosols), and fine-grained to pebbly sandstone (Milici 1974; Milici et al. 1979; Caudill et al. 1992, 1996; Driese et al. 1998). The Pennington Formation thins from east to west, and the terrigenous clastic content (relative to carbonate) also decreases in this

same direction; both trends reflect the demise of a late Mississippian carbonate shelf due to influx of terrigenous clastic sediment from the east. Within the study area the Pennington gradationally overlies the Bangor Limestone (Algeo and Rich 1992), and is disconformably overlain by the basal Pennsylvanian deposits of the Gizzard Group, chiefly the Raccoon Mountain Formation (Churnet 1996; Hurd and Stapor 1997). The depositional environments of the Pennington Formation include peritidal and coastal mudflat/sabkha environments, punctuated by periods of subaerial exposure and pedogenesis (Caudill et al. 1992, 1996), and terminated by paleokarst formation towards the end of Mississippian time (Driese et al. 1998; Humbert 2001).

The limestone deposits comprising the uppermost Pennington Formation are 4-6 m in aggregate thickness and are commonly arranged into an overall shoaling-upward package that consists of, in ascending stratigraphic order: (a) bioturbated skeletal packstone to wackestone (30-40 cm), (b) bioturbated peloidal wackestone to packstone (70 –130 cm), and (c) bioturbated to laminated and cross-stratified, skeletal grainstone to packstone (150-170 cm). Skeletal allochems are dominated by echinoderms, but also include brachiopods, bryozoans, mollusks (both pelecypods and gastropods), ostracodes, foraminifera, oncoid grains, calcispheres, and *Girvanella* tubules. Peloids and intraclasts are also common, and increase in abundance upsection. The amount of micritized rims and completely micritized grains increases upsection. Both inter- and intraparticle porosity increases upsection, as does the percentage of pore-filling calcite spar cement. Localized reddening occurs in the upper 5-15 cm of the uppermost limestone lithofacies, due to hematite coatings and impregnations of allochem grains.

The paleokarst surface that separates upper Pennington Formation limestone strata from overlying Pennsylvanian sandstone deposits has up to 3-4 m of demonstrable relief, as evidenced by laterally persistent strata that are truncated by paleokarst structures. Upper Pennington Formation paleokarst structures were initially described by Driese et al. (1998), and then later mapped in detail by Humbert (2001), who described three scales of features. Macroscale structures include paleo-dolines (i.e., paleo-sinkholes), the largest of which has a width of approximately 30m, and a depth of 4m. Other features include shallow and flat-floored karstic

depressions known as kamenitza, including the largest with a width of 7m and a depth of only 0.5m, and basal Pennsylvanian sandstone strata deformed by synsedimentary cave collapse in underlying limestone strata. Mesoscale features include mantling limestone breccia and conglomerate, red and greenish-gray claystone paleosols, vertical fissures filled with calcite spar cement, and iron oxide and oxy-hydroxide crusts. Microscale features, described in a subsequent section of this paper, include meteoric cements, grain micritization, reddening of the limestone, and extensive moldic pore development. Overlying Pennsylvanian sandstone strata contain a basal meter interval enriched in plant leaf, stem and log fossils that are carbonized, or "coalified," in layers up to 5 cm thick. Transported siderite pebbles are also locally abundant in the basal 1 m of Pennsylvanian sandstone.

Claystone paleosols locally mantle the paleokarst surface, especially in paleotopographic lows (see Driese et al. 1998, their Fig. 5C). One such prominent paleosol occurs at the Leatherwood Ford where it overlies weathered Pennington limestone that still retains some bedding and textural features (saprolite?; Fig. 1). The basal part of the profile is a platy 5R 2/6 clayshale, that grades upward into a blocky weathering claystone containing arcuate slickenside surfaces and root traces (Fig. 1A); the slickensides indicate shrink-swell processes associated with seasonal soil-moisture deficits (Wilding and Tessier 1988; Mora and Driese 1999). Cross-striated or stippled clay (sepic-plasmic) microfabrics are common in thin sections viewed under cross-polarized light and reflect periodic wetting and drying, which cause stress reorientation of clay matrix minerals (Blokhuis et al. 1990). Although perhaps all of the paleosol was initially red (10R 3/4) in color, the upper two-thirds of the blocky claystone was gleyed and converted to a drab gray-green (5Y 6/1) color, most likely upon burial by overlying basal Pennsylvanian strata (Fig. 1B, C). Color mottling is especially strong within the 1.1 to 1.3 m depth interval (Fig. 2A). The color mottling generally occurs as rinds around blocky claystone aggregates (Fig. 1B, C), and resembles some types of redoximorphic features interpreted in modern soils as evidence of seasonal cycles of saturation and aeration (Vepraskas 1994; Vepraskas and Guertal 1992). The drab gray-green claystone also contains spherules of hematite approximately 50-100 mm in

diameter (Fig. 1D), which have light-colored regions encircling each spherule. These hematite spherules morphologically resemble sphaerosiderite, as defined by Ludvigson et al. (1998), who interpret these as early-formed soil precipitates that indicate redox conditions intermediate between reducing and oxidizing formed in association with wet soil conditions.

METHODS

Three principal outcrop sections of the Pennington-Pennsylvanian stratigraphic contact were examined from the Kentucky-Tennessee border region (Leatherwood Ford Locality), and in east central Tennessee (Monterey and McMinnville Localities; Driese et al.1998, their Figs. 1, 2). Samples of limestone below the paleokarst surface were collected (see Driese et al. 1998 for full discussion). Thin-sections of collected samples were stained with Alizarin Red S and potassium ferricyanide (Dickson 1965; 1966) to identify dolomite and phases containing ferrous iron. Standard thin-section petrography was supplemented with cathodoluminescence (CL) petrography on a Technosyn luminoscope, using an accelerating potential of 10-12 KeV and beam current of 150-200 mA. Photomosaics (reflected light and CL) were prepared of sample areas selected for microprobe analysis.

Electron microprobe (EMP) analysis of over 400 points from seven different carbonate samples was performed on a Cameca SX-50 electron microprobe at the University of Tennessee. Calcite was analyzed by wavelength dispersive analysis using a 25 KeV accelerating voltage, 10 nA beam current, 10 mm beam spot diameter, and count times as follows: Ca (10 sec), Mg (20 sec), Mn and Fe (40 sec), and Sr (60 sec). Detection limits for these conditions at 99% confidence (3s) are (in wt.%): Mg (0.03), Mn (0.02), Fe (0.02) and Sr (0.03). Analytical uncertainty, based on Poisson distribution counting statistics and using appropriate carbonate standards, was determined to be $\pm$ 5% relative error for Ca, and $\pm$ 20% relative error for Mg, Fe, Mn and Sr.

Carbonate rocks were sampled for stable isotope analysis using a dental drill; average sample size was 3 mg. Carbon and oxygen isotope values were determined from CO_2 produced

by off-line reaction of powdered samples with 100% ortho-phosphoric acid after McCrea (1950). Isotopic ratios were determined using the VG 903 MM gas-source mass spectrometer at the University of Tennessee. Results are reported in standard-per mil (‰) notation relative to PDB with a reproducibility of $\pm$ 0.05 ‰.

Samples were collected at 10-20 cm intervals from claystone paleosol horizons for bulk quantitative chemical analysis using an EG & G ORTEC Tube-Excited Fluorescence Analyzer and high-Fe shale standards at the University of Tennessee. Bulk density was determined by paraffin coating of air-dried paleosol clods (Blake and Hartge 1986). Clay mineralogical analyses were performed using a Siemans D500 x-ray diffractometer and Ni-filtered Cu Ka radiation. Tube current and voltage were 30 mA and 40 Kev, respectively.

Whole-rock XRF chemical data were evaluated using a mass-balance approach, following Brimhall et al. (1988; 1991a; b), Driese et al. (2000), and Ashley and Driese (2001). This approach evaluates chemical variations in a soil or paleosol due to (1) the closed-system effects of residual enrichment and volumetric changes in the soil matrix and (2) open-system transport of material into or out of the soil. These values can be determined without making a direct volume measurement; only element concentration and bulk density measurements are necessary. This approach is appropriate for this study because it permits quantification of net gains and losses of Fe, a major element in paleosols mantling the paleokarst surface and also present in pore-filling cements in underlying Pennington limestone deposits. Uncertainties in the mass-balance methodology mainly arise in these three assumptions: 1) correct identification of parent material for the paleosol is established, 2) there were no significant additions to the parent material during pedogenesis, and 3) an immobile index element (typically Ti or Zr) can be identified. The reader is referred to the above original papers for complete development of pertinent equations and details on methodology.

PETROGRAPHY OF DIAGENETIC CALCITE

The general paragenetic sequence of pore-filling carbonate phases was previously

introduced (Driese et al. 1998, their Table 2) and illustrated (Driese et al. 1998, their Figs. 7, 8). There is no evidence such as pendant or meniscus cement to support that any of these cements formed in a vadose setting. In the overlying Pennsylvanian sandstone there is a lack of calcite cement, thereby making a comparison of the diagenesis below versus above the paleokarst surface difficult. The types of diagenetic features below the paleokarst surface, as well as their relative time-order, are consistent over the entire study area. There are three major types of diagenetic calcite as discussed by Driese et al. (1998), which include in order of their formation: (1) a dull luminescent, nonferroan calcite cement (DNF cement); (2) a concentrically banded luminescent-nonluminescent (BL cement), nonferroan calcite cement; and (3) a dull luminescent (DF cement), ferroan calcite cement. These phases of diagenetic calcite are followed by an episode of zoned siderite formation with a final generation of late vein-filling calcite cement. Below is a brief description of Pennington limestone diagenetic carbonate phases (also see Driese et al. 1998).

Primary Pore-Occluding Calcite Cements

DNF Cement. - The earliest cement, primarily precipitated on allochem grain surfaces, is a dull luminescent, nonferroan calcite cement (DNF cement in Fig. 3). In transmitted light, DNF cement ranges in appearance from clear to turbid. Additionally, the crystal morphology of DNF cement varies depending upon the nucleation substrate. DNF cement nucleated on echinoderm grains will typically develop into turbid syntaxial overgrowths (Walker et al. 1990). Conversely, formation on other carbonate phases results in a prismatic to columnar morphology (Wilson and Palmer 1992), with either a clear to turbid appearance and crystal lengths of only 20-30 μm. Although in general DNF cement is dully luminescent, particularly turbid DNF cement can exhibit a somewhat non-uniform or patchy appearance in CL, with patches varying in CL intensity from background dully luminescent cement (Fig. 3C, D).

BL and DF Cements. - In transmitted light, BL cement resembles later-formed DF

cement. Both of these cements have a water-clear appearance and consist of equant-shaped calcite crystals, which occlude both inter- and intra-granular primary pore spaces (Fig. 3A). Equant calcite exhibits a drusy fabric with a general increase in crystal size toward the center of occluded pore space. Equant calcite crystal size ranges from less than 0.1 mm along rims to greater than 1 mm in the center of occluded primary pores.

In terms of CL, BL cement exhibits a distinct banded appearance (Fig. 3B, C). The initial band is nonluminescent, and is generally followed by 3 to 7 concentric microbands that alternate between very bright and nonluminescent cement. Although the microbands in BL cement are correlatable within a single sample, intersample correlations of microbands are difficult. Conversely, DF cement is generally dully luminescent (Fig. 3B), which may exhibit a distinct sector zoning; earlier zones are dull luminescent, whereas the latest zones are nonluminescent. Unlike BL cement, DF cement may also occlude vertical fissure pores.

Late, Accessory Diagenetic Phases

Zoned siderite is locally present in the upper 10-15 cm of Pennington Formation limestone deposits (proximal to the paleokarst surface) at both the Leatherwood Ford and McMinnville outcrop sections. This phase is commonly associated with hematite impregnation and micritization of limestone. Siderite forms rhombs that are 0.05-0.10 mm wide and consist of a nonluminescent siderite core, followed by a very bright luminescent ferroan calcite overgrowth, which is in turn followed by a non-luminescent siderite overgrowth (Fig. 4A, B). The siderite is replacive and crosscuts all other petrographic constituents (DNF, BL, and DF cement), with the exception of late vein-filling cement. Late vein-filling cement is a very bright luminescent, ferroan calcite cement that occludes both fracture and intercrystalline porosity. Because this cement crosscuts all other petrographic constituents, it is interpreted as the latest diagenetic feature.

Stabilized Echinoderm Grains

Echinoderm grains are present in most Pennington Formation limestone deposits (Fig. 4C, D). Immediately below the paleokarst surface echinoderms are heavily stained by iron oxides and exhibit varying degrees of partial dissolution, replacement, and internal cementation. The CL of Pennington echinoderm grains is quite variable even at the scale of EMP analysis. Basically, echinoderm ossicles consist of primary skeletal calcite and a network of micropores, which was subsequently occluded with calcite cement. In CL skeletal calcite exhibits a generally dull luminescent appearance with some areas that are bright luminescent (Fig. 4D). Micropores were occluded by calcite that is mostly nonluminescent (Fig. 4D) and therefore most similar to BL cement.

GEOCHEMISTRY

Minor Element Composition of Calcite Cements and Echinoderm Grains

Primary Pore-Occluding Calcite Cements. **-** The Mg concentrations in DNF cement are somewhat variable. Concentrations of Mg in DNF cement from the McMinnville and Monterey localities are low (below detection limit to 2400 ppm; Table 1) versus Mg in DNF cement from the Leatherwood Ford locality, which is significantly higher (2800 to 5700 ppm; Table 1). However, DNF cement from all localities have low concentrations of Mn and Fe, particularly when compared with DF cement (Mn = below detection limit to 700 ppm; Fe = below detection limit to 1300 ppm; Table 1), with a many analyses below analytical detection limits for these elements.

Like DNF cement, the Mg concentrations of BL cement are generally higher at the Leatherwood Ford locality (400 to 3700 ppm; Table 1; Fig. 5A) versus the McMinnville locality (below detection limit to 1100 ppm; Table 1). Additionally, Fe values in BL cement are low at both of these localities (below detection limit to 1300 ppm; Table 1; Fig. 5A), with many analyses below the analytical detection limit. However, Mn values in BL cement are more variable at the Leatherwood Ford and McMinnville localities, ranging from below detection limit

to 7100 ppm (Table 1). Elevated Mn values in BL cement correspond to bright luminescent microbands.

The Mg in DF cement from all localities exhibit variable values of Mg (500 to 2800 ppm; Table 1) and Mn (below detection limit to 3700 ppm; Table 1). However, Fe values in DF cement are elevated when compared with either DNF or BL cements (1300 to 11200 ppm; Table 1). Late vein-filling, bright luminescent, ferroan calcite cement is characterized by low Mg (below detection limit to 600 ppm; Table 1), but high concentrations of Mn (2500 to 3900 ppm; Table 1) and Fe (2500 to 4200 ppm; Table 1).

Stabilized Echinoderm Grain. - Microprobe analyses of echinoderm grains from the Leatherwood Ford locality document spatial variability in Mg and Fe values as a function of distance from the paleokarst surface. Echinoderm ossicles located 400 cm below the paleokarst have elevated Mg (1500 to 2800 ppm; Fig. 5B; Table 1) compared with grains present within 30 cm of the paleokarst surface (400 to 2000 ppm; Fig. 5B; Table 1). Conversely, echinoderm grains located at the paleokarst surface tend to have higher Fe values (300 to 4600 ppm; Fig. 5B; Table 1) compared with samples collected significantly below the paleokarst surface (below detection limit to 1700 ppm; Fig. 5B; Table 1)

Stable Isotopes of Echinoderms and Selected Calcite Cements

A cross-plot of $\delta^{13}C$ versus $\delta^{18}O$ values of echinoderm grains exhibits a distinctive pattern of covariation. Echinoderms have variable $\delta^{13}C$ (Fig. 6; mean $\delta^{13}C$ = -0.5 ‰; -2.2 to 0.7 ‰ PDB) and less variable $\delta^{18}O$ values (Fig. 6; mean $\delta^{18}O$ = -5.9 ‰ PDB; -6.6 to -5.2 ‰ PDB). Additionally, Pennington echinoderm grains have $\delta^{13}C$ and $\delta^{18}O$ values that are considerably more negative than Mississippian marine calcite values (Meyers and Lohmann 1985; Popp et al. 1986). Note that the inset in Fig. 6 shows a distinct trend with depth for echinoderms from the McMinnville locality with increasing $\delta^{13}C$ values positively correlated with depth below the top of the paleokarst surface. DF calcite cement exhibits significantly more negative $\delta^{18}O$ values,

ranging from -11.9 to -7.6 ‰ PDB, and highly variable, but generally lower $\delta^{13}C$ values, ranging from -4.0 to 0.6 ‰ PDB (n = 24; mean $\delta^{18}O$ = -10.7 ‰ PDB; mean $\delta^{13}C$ = -1.3 ‰ PDB).

Paleosol Geochemistry

Alkali and alkaline earth elements, including Na, Ca, Mg, and Sr experienced 25-75% net gains in the paleosol (Fig. 2B). Si is relatively conserved (Fig. 2B) whereas Al exhibits 25% net gains in the paleosol. P shows a pattern characterized by net gains in the upper 40% of the paleosol, but with 10-25% net losses in the lower 120 cm. Redox-sensitive elements, including Mn, Fe and Cr, show net losses ranging from 80% for Mn (Fig. 2B) to 10-25% for Cr, with Fe losses averaging about 50% (Fig. 2B). Losses of redox-sensitive elements are positively correlated with the green-colored (5Y 6/1 to 5GY 5/1) portions in the upper 120 cm of the paleosol. All three redox-sensitive elements are conserved to slightly enriched in the basal 20 cm of the paleosol, which is characterized by red (5R 2/6) color. K, Ba, and Rb are enriched by 50-75% in the paleosol, with the highest enrichment corresponding with the 50-70 cm depth interval (Fig. 2B).

DISCUSSION

Evidence Supporting Echinoderm Stabilization by Meteoric Fluid

Field data from the limestone-dominated upper 4 to 6 m of the Pennington Formation indicate that the top of this unit is a surface of subaerial exposure and that the upper Pennington was affected significantly by pedogenesis and meteoric diagenesis (Driese et al. 1998; Humbert 2001). The large-scale dissolution of carbonate phases, forming paleodolines, paleocaverns, kamenitzas, rundkarren, carbonate clast breccia, and vertical dissolutional fissure, suggests alteration of marine limestone by interaction with meteoric water that was undersaturated with respect to metastable carbonate phases. Similar features are associated with other Mississippian paleokarst intervals (Wright 1982; Esteban and Klappa 1983; Meyers 1988; Sando 1988; Hattin and Dodd 1992).

Ancient echinoderm skeletons are commonly inferred to have a metastable, high-Mg calcite original mineralogy (Wilkinson 1979) and are therefore highly susceptible to diagenetic alteration and stabilization to a mixture diagenetic low-Mg calcite and microdolomite (Lohmann and Meyers 1977). Additionally, echinoderm skeletal material is highly porous and extensive occlusion of these pores by diagenetic calcite is common (Dickson 1995). Stabilization commonly imposes the diagenetic signature of the stabilizing fluid on to the altered metastable component. Consequently, despite the original marine diagenetic environment in which echinoderm ossicles were formed, there is a high likelihood that a later diagenetic signature will be imparted on to these grains. Given the overwhelming field evidence, cited above, for subaerial exposure immediately above the Pennington limestone, the inference is made that Pennington echinoderm grains were stabilized by meteoric fluids associated with the overlying paleokarst.

Echinoderm grains exhibit a distinct covariation of $\delta^{13}C$ and $\delta^{18}O$ values, which is characterized by variable $\delta^{13}C$ and less variable $\delta^{18}O$ values (Fig. 6). Meyers and Lohmann (1985) and Popp et al. (1986) record Mississippian marine cement $\delta^{13}C$ (4 ‰ PDB) and $\delta^{18}O$ (-2 ‰ PDB) values that are significantly more positive than Pennington echinoderms. Using the Kim and O'Neil (1997) equation that defines the fractionation factor of oxygen isotopes between calcite and water, the oxygen isotopic composition of meteoric fluid can be calculated. Using a mean $\delta^{18}O$ = -5.9 ‰ PDB for calcite and assuming a temperature of 25 ^{o}C, a $\delta^{18}O$ value for meteoric water can be calculated, which is -3.6 ‰ SMOW. Carboniferous seawater likely was -1±1 ‰ SMOW (Hudson and Anderson 1989). Consequently, Pennington echinoderms must have been stabilized in meteoric water that was 2 to 4 ‰ more negative than coeval seawater, a relationship characteristic of low latitudinal settings (Dansgaard 1964). During the middle Carboniferous Tennessee was located at a low paleolatitude ($\approx$ 20 ^{o}S; Scotese and Golanka 1992). Therefore, the isotopic variation of Pennington echinoderms likely reflects a segment of a meteoric water line (Lohmann 1988). Additionally, similar relationships for Carboniferous isotopic values between coeval marine and calcite phases (e.g., laminar crusts) that are

unequivocally related to subaerial exposure of a paleokarst surface have been documented (Mutti 1994; Canaveras et al. 1996).

Additionally, there is a distinct depth trend associated with echinoderm $\delta^{13}C$ values (inset in Fig. 6). The highest $\delta^{13}C$ values occur in the sample located 400 cm below the paleokarst surface versus samples at and immediately below the top of the paleokarst surface that have significantly the lower $\delta^{13}C$ values. This observation is consistent with a greater extent of alteration localized immediately below the paleokarst surface as aggressively undersaturated (with respect to calcite) meteoric fluid infiltrated into the Pennington limestone. At depth below the paleokarst surface less intense alteration results in echinoderm $\delta^{13}C$ values that are closer to the Mississippian marine value.

Origin of Elevated Fe Content of Echinoderm Grains Adjacent to the Paleokarst Surface

The elevated Fe concentrations present in echinoderm grains immediately adjacent to the paleokarst surface are unequivocally the consequence of diagenetic alteration of these metastable grains (high-magnesium calcite; Wilkinson 1979). Indeed, with increasing diagenetic alteration Fe content tends to increase (Veizer 1983). Presence of Fe-rich echinoderms implies that the meteroic fluid along the paleokarst surface, which was responsible for echinoderm stabilization, was anaerobic with elevated Fe concentrations. Redox (Fe) depletions and sphaerosiderite present in the paleosol indicate early formation of gley (water-logged, reducing) conditions within the overlying paleosol. Therefore, a likely source for Fe in the echinoderms was the reduction of Fe-oxyhydroxides in paleosol material immediately above the Pennington limestone, with subsequent removal of Fe from the paleosol and sequestration of Fe in diagenetic calcite phases present in subjacent limestone. Depletion of Fe in the upper paleosol (Fig. 6B) and concentration of Fe in echinoderm grains, especially, echinoderms immediately below the paleokarst surface that is draped with paleosol deposits (Fig. 2B), supports the above inference. The substantial losses of redox-sensitive elements, including Mn, Fe and Cr (Fig. 6B), which correlates positively with drab gray-green paleosol colors (5Y 6/1 to 5GY 5/1), implies

mobilization of these elements, presumably due to post-burial reductive process. Modern Vertisols and paleoVertisols rarely experience total Fe losses of this magnitude (Driese et al. 2000; S. Driese and C. Mora, pers. comm.).

What process can facilitate the redox transfer of Fe from the oxidized (paleosol) to the reduced (calcite) state? Thermochemical reduction of Fe from paleosols in the burial diagenetic realm is not consistent with low temperature, near-surface diagenetic setting of echinoderm stabilization supported by the evidence presented in the previous section. Fe reduction at near surrface temperatures could be either abiotic or microbially mediated. Given the antiquity of Pennington deposits unequivocally establishing a microbial-geochemical connection would be extremely difficult. Even in modern groundwater systems documentation of this connection is not a trivial task. Therefore, we can not prove that paleosol Fe reduction was microbial mediated. We can offer some circumstantial evidence that supports microbial mediated transfer of Fe from the paleosol to subjacent limestone. (1) Microorganisms are ubiquitous in the shallow subsurface of the Earth's lithosphere (Parkes et al. 1994). (2) Fe-reducing bacteria have been isolated and characterized from modern sedimentary systems (Lovley 1991). (3) Iron reduction is commonly coupled to the respiration of organic material in low Eh settings. At the Leatherwood Ford section significant coal lenses occur immediately above the paleokarst surface providing a source of organic material. Coal lenses are present at McMinnville, but not as close to the contact as at Leatherwood Ford. Additionally, localized root traces within the paleosol provide another possible source for organic material. Consequently, organic material could have served as potential electron donors facilitating microbial Fe reduction of Fe-oxyhydroxides in the paleosol. It has been demonstrated that natural organic material not only facilitates but indeed enhances bioreduction of hematite (Royers in press).

Modeling Fluid Composition Responsible for Echinoderm Stabilization

The goal of this section is to better constrain the minor element and stable isotopic composition of the meteoric fluid that stabilized the Pennington echinoderms. We will use the

computer program PHREEQC (Parkhurst and Appelo 1999) to determine carbonate solubility indexes (SI) for various fluids that could have facilitated the stabilization of Pennington echinoderm grains. Fluids must have been undersaturated with respect to calcite if stabilization occurred. Additionally, we will model the stable isotopic and minor element compositional evolution of Pennington echinoderm grains during stabilization using the approach of Banner and Hanson (1990). The objective is to determine a meteoric fluid composition consistent with observed minor element and stable isotopic data for Pennington echinoderms.

Step #1 - Assuming a Baseline Meteoric Fluid - There is no unique soil water chemistry characteristic to vertisols; but, rather soil water chemistry varies greatly with climate, topography, and parent material. Hence, we select modern river water (Mg = 3.8 ppm; Ca = 14.6 ppm; Drever, 1997) as a starting point for our modeling realizing that Pennington meteoric water may have had a substantially different composition. To achieve solution charge balance for baseline meteoric fluid we assume that the equivalent negative charge present in our baseline meteoric fluid is in the form of dissolved inorganic carbonate (DIC) species.

(1) $Mg^{2+} + Ca^{2+} =$ Carbonate Alkalinity (DIC)

Mg-Ca-bicarbonate meteoric water is common in regions with limestone bedrock (Appelo and Postma 1996) such as the Pennington paleokarst surface (Fig. 7). Initial aqueous carbonate speciation is constrained by ambient mid-Carboniferous pCO_2 level. During this time period Berner (1997) has modeled pCO_2 levels at < 4 of present atmospheric level (PAL; Berner, 1997). Indeed results from Pennington paleosols in indicate atmospheric pCO_2 = 2 to 3 PAL (Mora *et al.,* 1996). Hence, we suggest that Pennington meteoric was initially in contact with an atmospheric pCO_2 = 2 PAL. Sensitivity of calcite SI is minimal with varying pCO_2 values in the above range.

Step #2 – Modeling Heterotrophic Consumption of pO_2. - Pennington echinoderm grains have Fe concentrations, which is suggestive of stabilization under anaerobic conditions. Consequently, ambient dissolved oxygen, derived from contact with the mid-Carboniferous atmosphere, that was present originally in baseline meteoric fluid must have been consumed; likely by microbial heterotrophy (see above arguments). Impact of oxygen consumption on solution chemistry was modeled with PHREEQC assuming the coupling organic material to the consumption of all dissolved oxygen (DO = 0.3 mM; reaction #2).

(2) $CH_2O + O_2 \rightarrow H_2CO_3$

The net result of reaction 2 was to decrease calcite solubility and solution pH and increase DIC.

Step #3 – Modeling Fe Reduction. - Next, as anaerobic conditions are established with the consumption of all DO, alternative electron acceptors were likely utilized by existing microbial populations. Paleosols overlying the paleokarst surface contains an abundance of ferric iron that could have been coupled with organic material driving anaerobic microbial respiration (reaction #3), which was modeled with PHREEQC.

(3) $2\,Fe_2O_3 + CH_2O + 3\,H_2O \rightarrow 4\,Fe^{2+} + HCO_3^- + 7\,OH^-$

Reaction 3 causes an increase in calcite SI, solution pH, and DIC ($C_{f,o}$). Water associated with gleying in modern soils tends to have concentrations of ferrous iron near 1 ppm (Vepraskas and Wilding 1983; Vepraskas and Guertal 1992). Therefore, three solutions, low (Fe^{2+} = 0.25 ppm; River Water A), intermediate (Fe^{2+} = 1 ppm; River Water B) and high (Fe^{2+} = 4 ppm; River Water C), were modeled with PHREEQC. Significant calcite undersaturation (saturation index, SI < 0) was noted only for solutions that have lower ferrous iron concentrations with excessive Fe reduction yielding solutions that are closer to calcite saturation (Table 2), which is

inconsistent with echinoderm stabilization.

Step #4 - Modeling Fluid-Rock Interaction of Echinoderm Stable Isotopes. - To model fluid-rock interactions associated with echinoderm stabilization we used the equations originally presented by Banner and Hanson (1990). For all calculations an open system is assumed with a pre-DF cement porosity present in the uppermost Pennington limestone of 30% (Banner and Hanson 1990; see their equation 4) and a temperature of 25 °C.

For the $\delta^{18}O$ system the fractionation factor used is that of Kim and O'Neil (1997) and by assuming a temperature of 25 °C, $\alpha_{Calcite\text{-}H2O}$ was constrained (Table 3). As indicated above, the $\delta^{18}O$ value of meteoric water ($\delta_{f,o}$) at this temperature was calculated at -3.6 ‰ SMOW (Table 3) and Meyers and Lohmann (1985) and Popp et al. (1986) record Mississippian marine cement with $\delta^{18}O$ = -2 ‰ PDB, which we used as an initial marine calcite value ($\delta_{calcite,o}$) to begin iterative calculations (Banner and Hanson 1990; see their equations 24 and 25). The $\delta^{18}O$ value of echinoderms was rapidly altered by meteoric water (Fig. 6) and essentially after only modest degrees of interaction (cumulative fluid-rock ratio N < 10) echinoderm $\delta_{calcite}$ values converged on an equilibrium value of -5.9 ‰ PDB, which is a characteristic of a meteoric water line (Lohmann 1988).

When modeling the $\delta^{13}C$ isotopic system fractionation it is important to consider the fractionation between various aqueous carbonate species and calcite. Fortunately, at step #3 solution pH (as determined by PHREEQC speciation modeling, Table 2) the dominant carbonate species was likely to have been HCO_3^-. Romanek et al. (1992) indicated that there is minimal fractionation between aqueous HCO_3^- and calcite, and hence note the low ($\alpha_{Calcite\text{-}H2O}$) value used in the calculations (Table 3). Finally, the meteoric water carbon isotopic value ($\delta_{f,o}$; Table 3) is assumed to reflect an equal mixture of carbon derived from organic matter (^{13}C = -26 ‰ PDB; Mora et al. 1996) and derived from stabilizing and dissolving marine limestone phases (4 ‰ PDB), which define the initial marine calcite value ($\delta_{calcite,o}$).

Using the above-selected input parameters for the $\delta^{13}C$ isotopic system iterative

modeling of echinoderm stabilization (using the approach of Banner and Hanson 1990) required significant fluid-rock interaction to achieve observed echinoderm $\delta^{13}C$ values (Fig. 6). Note that the cumulative fluid-rock values (N) is broadly constrained between1000 to 5000 (Fig. 6). Cumulative fluid-rock values derived from iterative calculations are highly insensitive to variable ($C_{f,o}$) values when < 25 ppm of C.

Step #5 - Modeling Fluid-Rock Interaction of Echinoderm Minor Elements. - Echinoderm skeletons are commonly inferred to have a metastable, high-Mg calcite original mineralogy (Dickson 1995). As echinoderm grains are stabilized with progressive fluid-rock interaction Mg values should decrease ultimately reaching an equilibrium baseline with increasing Fe (Veizer 1983).

Table 4 lists the parameters needed to model the impact of fluid-rock interaction (Banner and Hanson 1990) on echinoderm Mg and Fe values. Echinoderm skeletons are commonly inferred to have a metastable, high-Mg calcite original mineralogy (Dickson 1995) so that the initial Mg content of echinoderm grains Mg ($C_{calcite,o}$) was assumed to have been 12 wt % Mg (Table 4). Inspection of Fig. 2B indicates that Mg values achieved a baseline equilibrium at near 1200 ppm. Consequently, we assumed that Mg ($C_{calcite,e}$) = 1200 ppm (Table 4). Fluid Mg values Mg (C_f) for each modeled fluid are obtained from Table 2. Iterative modeling of Mg was achieved using equations 3, 7, and 10 from Banner and Hanson (1990).

For Fe, fluid-rock calculations are insensitive initial calcite Fe concentration Fe ($C_{calcite,o}$) and calculations begin with an Fe value of 2 ppm (Table 4; Veizer 1983). The lowest experimental Fe (K_D) value for calcite at 25 ^oC is 1.9 (Table 4; Dromgoole and Walter 1990), which is associated with very slowly precipitating calcite. Echinoderm stabilization proceeded with fluids circulating within the micro-porosity network present in the ossicle. In such a restricted diagenetic setting reactant supply (Ca^{2+}; HCO_3^-) and new calcite formation was likely limiting during stabilization unlike diagenetic settings that experience much more rapid crystal growth (e.g. beach rock; speleothems in caves) where selection of higher Fe (K_D) might be

warranted. Consequently, calcite formation - alteration associated with echinoderm stabilization was likely very slow, thereby justifying the selection of a low Fe (K_D) value. Fluid Ca (Ca_f) and Fe (C_f) values are prescribed for each modeled diagenetic fluid (Table 2). Iterative modeling of Fe utilized equations 2, 3, and 7 from Banner and Hanson (1990).

The ultimate objective is to determine a calculated composition from iterative modeling of Mg and Fe that best matches observed Pennington echinoderm Mg and Ca values. An additional constraint is the iterative modeling of $\delta^{13}C$ and $\delta^{18}O$ values that indicates that the cumulative fluid-rock values (N) was likely between1000 to 5000 (Fig. 4). Fig. 7 shows calculated fluid-rock interaction curves for three fluids (River Water A, River Water B, River Water C). Fluid-rock interaction curve for River Water C (Fe (C_f) = 4 ppm) does not match observed Pennington echinoderm Mg and Fe concentrations; additionally note that this fluid is nearly saturated with respect to calcite (Table 2) and hence is not a good model composition for a Pennington meteoric fluid that facilitated echinoderm stabilization. Fluid-rock interaction curve for River Water A (Fe (C_f) = 0.25 ppm) better matches Pennington echinoderm Mg and Fe values. However, extremely high N (> 5000) values, inconsistent with $\delta^{13}C$ and $\delta^{18}O$ iterative modeling, are needed to account for the elevated Fe concentrations of echinoderm immediately below the paleokarst. Best match is achieved with River Water B, which has Fe (C_f) values most similar to modern gley soils (1 ppm).

Sensitivity Check. - Varying DIC content and Mg/Ca ratio. - To see if a unique result has been obtained different baseline meteoric fluids were modeled (steps # 1 to 5) as described above. Four different series of solutions with varying step #1 DIC concentrations were considered (Series 1 = 3.1 ppm of C; Series 2 = 6.2 ppm of C; Series 3 = 12.5 ppm of C; Series 4 = 25.0 ppm of C; Table 2). Additionally, for each series fluids with three different Mg/Ca ratios typical of meteoric systems (Morse and Mackenzie 1990) were modeled (A = 0.25; B = 0.5; C = 1.0; Table 2). For these calculations an Fe (C_f) value = 1 ppm was assumed.

All solutions modeled are undersaturated with respect to calcite (Table 5) and hence

could possibly facilitate echinoderm stabilization. With increasing DIC content calculated calcite SI (from step #3) increases. Consequently, echinoderm stabilization is inconsistent with excessive DIC values (>> 25 ppm of C), which decreases calcite solubility resulting in saturated to supersaturated solutions with respect to calcite. Additionally, siderite supersaturation associated with Series 4 solutions is inconsistent with the lack of early diagenetic siderite in the uppermost Pennnington limestone deposits suggesting that DIC concentrations were < 25 ppm of C. Siderite in uppermost Pennington limestone cross-cuts DF cement and is likely burial in origin (Driese et al. 1998).

Figs. 8 and 9 shows calculated fluid-rock interaction curves for the four series of solution compositions described above. At extremely low DIC concentrations (Series 1; Fig. 8A) fluid-rock interaction curve determined from iterative modeling of Mg and Fe does not match observed Pennington echinoderm Mg and Fe concentrations. At slightly higher DIC concentrations (Series 2; Fig. 8B) match is achieved only if a high Mg/Ca ratio (1) is assumed. Overall, series 3 and 4 (Fig. 9) fluid-rock interaction curve better matches observed Pennington echinoderm Mg and Fe. However, cumulative fluid-rock values (N) determined from Mg and Fe iterative modeling of series 3 solutions better matches N values determined by iterative modeling of $\delta^{13}C$ and $\delta^{18}O$ values than series 4 solutions (Fig. 9). Series 4 (Fig. 9B) which show correspondence between fluid-rock interaction curve and observed Pennington echinoderm Mg and Fe concentrations when N < 1000.

In conclusion, the above model results are consistent with a composition for the fluid that facilitated Pennington echinoderm stabilization that is similar to modern river water that was modified by anaerobic microbial processes in a soil gley setting. While it is not possible to determine the exact composition of the echinoderm stabilizing fluid the above results provide strong support for alteration of echinoderm grains in a meteoric diagenetic milieu.

Development of Paleokarst Surface

The morphology of the paleokarst surface was described in a previous section of this

paper. The development of the paleokarst surface can be ascribed to five stages (Humbert 2001) as is illustrated in Fig. 10 with additional insights based on geochemical modeling as discussed above.

Stage 1: Paleokarst began with subaerial exposure of subtidal Pennington Formation limestone deposits, which comprise a 3-4 m thick shoaling-upward succession described in a previous section of this paper. Dissolution initiated along vertical fractures or channels (grikes), that gradually enlarged in width and depth, due to interaction with aggressive meteoric water. Echinoderm grains began stabilization, and substantial grain-moldic and interparticle porosity likely developed during this stage (*e.g.* River Water B; Calcite SI = -0.4 after completion of only step #1).

Stage 2: A packet of red, silty claystone was deposited on top of the dissolving limestone, and a plant community was established in the soil that gradually formed. Solution channels beneath the soil mantle were enlarged both laterally and vertically to form flat-floored, <0.5 m deep by 2-5 m wide kamenitza, and 2-4 m deep by 5-10 m wide dolines. Paleokarst breccias formed on the edges of paleodolines, and were incorporated into paleodoline-paleosol infillings. Poor drainage and seasonal water-table perching in some of the paleodolines initiated minor development of surface gley and redoximorphic features, although soil conditions were overall well-drained and oxidizing. Sphaerosiderite (later pseudomorphed to hematite) began to form in the clay matrix within the paleosol. Presence of sphaerosiderite was likely due to microbial Fe reduction resulting in locally elevated ferrous iron concentrations (*e.g.* River Water C; Siderite SI = 1.3; Table 5). Oxic conditions present in subjacent limestone favored localized oxidation of ferrous iron and formation of an Fe-oxyhydroxide rind that impregnated the uppermost 2-5 cm of Pennington limestone deposits.

Stage 3: Additional siliciclastic material (mainly siltstone and shale) and organic C (plant remains) was deposited augmenting existing red paleosol material, and burying Pennington limestone bedrock highs. Additionally, limestone breccia clasts were sled from the margins of paleokarst highs into adjacent paleotopographic lows.

Stage 4: Additional gray-colored siliciclastic material (mainly siltstone and shale deposits, but also including thin sandstone layers) and organic C (plant remains) of either Late Mississippian or Early Pennsylvanian age were deposited in a fluvio-deltaic setting on top of stage 3 siliciclastic deposits. Eventually, paleocaverns in the Pennington limestone deposits collapsed, thus causing localized foundering of overlying unconsolidated Upper Mississippian or Lower Pennsylvanian siliciclastic sediments. Deformed sandstone, siltstone and shale deposits, with near-vertical bedding orientations, mark the edges of these major collapse features. Drainage on the irregular karstic surface became impeded. Burial gley features influenced the paleosol, as organic matter began to be respired, and microbial reduction of Fe commenced. Confined phreatic conditions were established in the paleosol and underlying limestone due to rising water table, and reduced Fe began to be incorporated within stabilizing echinoderm grains (*e.g.* River Water B; Calcite SI = -1.1; Table 5).

Stage 5: Lower Pennsylvanian estuarine siltstone and shale deposits of the Raccoon Mountain Formation were deposited on top of the karstic surface, burying the topography, and depositing reworked siderite pebbles and plant debris. The Warren Point Sandstone (Lower Pennsylvanian) was then deposited as part of a sandy braidplain complex (Hurd and Stapor 1997). A general hydrogeologic system was established in which the Warren Point Sandstone served as a paleoaquifer; the underlying paleosol functioned as the aquitard, and the Pennington limestone deposits behaved as a semi-confining unit. Additional burial gley developed in the paleosol due to poor internal drainage in the paleosol and oxidation of organic C, and reduced Fe may have been incorporated within stabilizing echinoderm grains.

SUMMARY

The stabilization of metastable phases within the Pennington limestone, which lies below a paleokarst surface defining the Mississippian-Pennsylvanian boundary in Tennessee, is likely to have been facilitated by reducing meteoric fluid. Covariation of $\delta^{13}C$ and $\delta^{18}O$ echinoderm values supports the premise of echinoderm stabilization by meteoric fluid. Alteration of

echinoderm grains is most intense immediately below the paleokarst surface as reflected by low Mg and elevated Fe concentrations.

Deposition of plant material immediately above the paleokarst surface provided organic material. Microbial respiration of this organic matter likely could have been driven by the presence of electron acceptors (such as Fe) that resided within the paleosol. Therefore, elevated concentrations of Fe in stabilized echinoderm grains immediately below the paleokarst surface could reflect the ultimate sink for microbially reduced Fe. Quantitative modeling of carbonate solubility (PHREEQC) and iterative modeling of calcite minor element and stable isotopic compositions support the above assertions.

ACKNOWLEDGMENTS

This research was supported by PRF Grant 25678-AC8-C, and by NSF Grants EAR-9206540, EAR-9418183, and EAR-9814607 awarded to S. Driese and C. Mora. C. Mora (Univ. of Tennessee) reviewed an earlier draft of this manuscript and her helpful comments are appreciated. Members of the Paleokarst Seminar Research Group helped with many aspects of this study: M. Caudill, S. Dunagan, B. Glumac, P. Milroy, T. Schultz, A. Stefaniak, R. Tolliver, and J. Williams. E. Humbert provided invaluable insights into field relationships at Leatherwood Ford. M. Caudill assisted with XRF analyses. I. Richards and A. Halleran assisted with stable isotopic analyses. A. Patchen facilitated microprobe analyses. We thank the National Park Service for granting us access to outcrop exposures in the Big South Fork National Recreation Area.

REFERENCES

Algeo, T.J., and Rich, M., 1992, Bangor Limestone: Depositional environments and cyclicity on a late Mississippian shelf: Southeastern Geology, v. 32, p. 143-162.

Appelo, C.A.J.,and Postma, D., 1996, Geochemstry, groundwater and pollution: Rotterdam, The Netherlands, A.A. Balkema, 536 p.

Ashley, G.R., and Driese, S.G., 2000, Paleopedology and paleohydrology of a volcaniclastic paleosol: Implications for Early Pleistocene paleoclimate record, Olduvai Gorge, Tanzania: Journal of Sedimentary Research, v. 70, p. 1065-1080.

Banner, J.L., and Hanson, G.N., 1990, Calculation of simultaneous isotopic and trace element variations during water-rock interaction with applications to carbonate diagenesis: Geochimica et Cosmochimica Acta, v. 54, p. 3123-3137.

Berner, R.A., 1997, The rise of plants and their effect on weathering and atmospheric CO_2: Science, v. 276, p. 544-546

Bjerg, P.L., Rugge, K., Pedersen, J.K., and Christensen, T.H., 1995, Distribution of redox-sensitive groundwater quality parameters downgradient of a landfill (Grindsted, Denmark): Environmental Science & Technology, v. 29, p. 1387-1394.

Blake, G.R., and Hartge, K. H., 1986, Bulk density, *in* Klute, A. (ed.), Methods of soil analysis part I . Physical and mineralogical methods: Soil Science Society of America, Agronomy, Monologue 9 (2nd edition), p. 363-375.

Blokhuis, W.A., Kooistra, M.J., and Wilding, L.P., 1990, Micromorphology of cracking clayey soils (Vertisols), *in* Douglas, L.A. (ed.), Soil micromorphology: A basic and applied science: New York, Elsevier Publishing Company, Developments in Soil Science 19, p. 123-148.

Brimhall, G.H., Lewis, C.J., Ford, C., Bratt, J., Taylor, G., and Warin, O., 1991a, Quantitative geochemical approach to pedogenesis: importance of parent material reduction, volumetric expansion, and eolian influx in lateritization: Geoderma, v. 51, p. 51-91.

Brimhall, G.H., Chadwick, O.A., Lewis C.J., Compston, W., Williams, I.S., Danti, K.J., Dietrich, W.E., Power, M., Hendricks, D., and Bratt, J., 1991b, Deformational mass transfer and invasive processes in soil evolution: Science, v. 255, p. 695-702.

Brimhall, G.H., Lewis, C.J., Ague, J.J., Dietrich, W.E., Hampel, J., Teague, T., and Rix P., 1988, Metal enrichment in bauxites by deposition of chemically mature aeolian dust: Nature, v. 333, p. 819-824.

Canaveras, J.C., Sanchez-Moral, S., Calvo, J.P., Hoyos, M., and Ordonez, S., 1996, Dedolomites associated with karstification: an example of early dedolomitization in lacustrine sequences from the Tertiary Madrid Basin, central Spain: Carbonates and Evaporites, v. 11, p. 85-103.

Caudill, M.R., Mora, C.I., Tobin, K.J., and Driese, S.G., 1992, Preliminary interpretations of paleosols associated with Late Mississippian marginal marine deposits, Pennington Formation, Monterey, Tennessee, *in* Driese, S.G., Mora, C.I., and Walker, K.R., eds., Paleosols, Paleoweathering Surfaces, and Sequence Boundaries: Field Trip Guidebook, Society for Sedimentary Geology Midcontinent Section, Volume 10: University of Tennessee, Department of Geological Sciences, Studies in Geology No. 21, 115 p.

Caudill, M.R., Driese, S.G., and Mora, C.I., 1996, Preservation of a paleo-Vertisol and an estimate of Late Mississippian paleoprecipitation: Journal of Sedimentary Research, v. 66, p. 58-70.

Churnet, H.G., 1996, Depositional environments of Lower Pennsylvanian coal-bearing siliciclastics of southeastern Tennessee, northwestern Georgia, and northeastern Alabama, U.S.A.: International Journal of Coal Geology, v. 31, p. 21-54.

Crawford, T.J., 1985, Upper Mississippian and Lower Pennsylvanian series in the southern Appalachians: United States Geological Survey, Open File Report 85-577, p. 9-10.

Dansgaard, W., 1964, Stable isotopes in precipitation: Tellus, v. 16, p. 436-468.

Dickson, J.A.D., 1965, Modified staining technique for carbonates in thin section: Nature, v. 205, p. 587.

Dickson, J.A.D., 1966, Carbonate identification and genesis as revealed by staining: Journal of Sedimentary Petrology, v. 36, p. 491-505.

Dickson, J.A.D., 1995, Paleozoic Mg calcite preserved - implications for the Carboniferous ocean: Geology, v. 23, p. 535-538.

Drever, J.I., 1997, The geochemistry of natural waters: surface and groundwater environments, Saddle River, New Jersey, Prentice Hall, 436 p.

Dromgoole, E.L., and Walter, L.M., 1990, Iron and manganese incorporation into calcite: effects of growth kinetics, temperature and solution chemistry: Chemical Geology, v. 81. p. 311-336.

Driese, S.G., Caudill, M.R., Srinivasan, K., 1998, Late Mississippian to Early Pennsylvanian paleokarst in east-central Tennessee: field, petrographic, and stable isotope evidence: Southeastern Geology, v. 37, p. 189-204.

Driese, S.G., Mora, C.I., Stiles, C.A., Joeckel, R.M., and Nordt, L.C., 2000, Mass-balance reconstruction of a modern Vertisol: Implications for interpretations of geochemistry and burial alteration of paleoVertisols: Geoderma, v. 95, p. 179-204.

Esteban, M., and Klappa, C.F., 1983, Subaerial exposure environment, *in* Scholle, P.A., Bebout, D.G., Moore, C.H., eds., Carbonate Depositional Environments: American Association of Petroleum Geologists, Memoir 33, p. 1-54.

Fredrickson, J.K., McKinley J.P., Bjornstad, B.N., Long, P.E., Ringelberg, D.B., White, D.C., Krumholz, L.R.,Suflita, J.M., Colwell, F.S., Lehman, R.M., Phelps, T.J., and Onstott, T.C., 1997, Pore-size constraints on the activity and survival of subsurface bacteria in a Late Cretaceous shale-sandstone sequence, northwestern New Mexico: Geomicrobiology Journal, v. 14, p. 183-202.

Hattin, D.E., and Dodd, J. R., 1992, Mississippian paleosols, paleokarst, and eolian carbonates in Indiana: Ohio Geological Survey, Miscellaneous Report No. 3, 35 p.

Hendry, J.P., 1993, Calcite cementation during bacterial manganese, iron and sulphate reduction in Jurassic shallow marine carbonate: Sedimentology, v. 40, p. 87-106.

Hudson, J.D., and Anderson, T.F., 1989, Ocean temperatures and isotopic compositions through time: Transactions of the Royal Society of Edinburgh, v. 80, p. 183-192.

Humbert, S.E., 2001, Subaerial paleokarst in upper Pennington Formation limestones (Upper Mississippian), Big South Fork Recreation Area, Tennessee [unpublished M.S. Thesis]: Knoxville, University of Tennessee, 143 p.

Hurd, S.A., and Stapor, F.W., Jr., 1997, Facies, stratigraphy and provenance of the Warren Point Sandstone, (Pennsylvanian), Cumberland Plateau, central Tennessee: Southeastern Geology, v. 36, p. 187-201.

Kim, S-T, O'Neil, J.R., 1997, Equilibrium and nonequilibrium oxygen isotope effects in synthetic carbonates: Geochimica et Cosmochimica Acta, v. 61, p. 3461-3475.

Lohmann, K.C., 1988, Geochemical patterns of meteoric diagenetic systems and their application to studies of paleokarst, *in* Choquette, P.W., and James, N.P., eds., Paleokarst: New York, Springer-Verlag, p. 58-80.

Lohmann, K.C., and Meyers, W.J., 1977, Microdolomite inclusions in cloudy prismatic calcites: a proposed criterion for former high-magnesium calcites: Journal of Sedimentary Petrology, v. 47, p. 1078-1088.

Lovely, D.R., 1991, Dissimilatory Fe(III) and Mn(IV) reduction: Microbiological Reviews, v. 55, p. 259-287.

Ludvigson, G.A., Gonzalez, L.A., Metzger, R.A., Witzke, B.J., Brenner, R.L., Murillo, A.P., and White, T.S., 1998, Meteoric sphaerosiderite lines and their use for paleohydrology and paleoclimatology: Geology, v. 26, p. 1039-1042.

McMahon, P.B., Williams, D.F., and Morris, J.T., 1990, Production and isotopic composition of bacterial CO_2 in deep coastal-plain sediments of South Carolina: Ground Water, v. 28, p. 693-702.

McCrea, J.M., 1950, On the isotopic chemistry of carbonates and a paleotemperature scale: Journal of Chemistry and Physics, v. 18, p. 849-857.

Meyers, W.J., 1988, Paleokarstic features on Mississippian limestones, New Mexico, *in* Choquette, P.W., and James, N.P., eds., Paleokarst: New York, Springer-Verlag, p. 306-328.

Meyers, W.J., and Lohmann, K.C., 1985, Isotope geochemistry of regionally extensive cement zones and marine phases in Mississippian limestones, New Mexico, *in* Schneidermann, N., and Harris, P.M., Carbonate Cements: SEPM, Special Publication No. 36, p. 223-239.

Milici, R.C., 1974, Stratigraphy and depositional environments of Upper Mississippian and Lower Pennsylvanian rocks in the southern Cumberland Plateau of Tennessee, *in* Briggs, G., ed., Carboniferous of the Southeastern United States: Geological Society of America, Special Paper No. 148, p. 115-133.

Milici, R.C., Briggs, G., Knox, L.M., Sitterly, P.D., and Statler, A.T., 1979, The Mississippian and Pennsylvanian (Carboniferous) Systems in the United States-Tennessee: U.S. Geological Survey Professional Paper 1110-G, 38 p.

Mora, C.I., and Driese, S.G., 1999, Palaeoclimatic significance and stable carbon isotopes of Palaeozoic red bed paleosols, Appalachian Basin, USA and Canada, *in* Thiry, M., and Simon-Coinçon, R. (eds.), Palaeoweathering, palaeosurfaces and related continental deposits: International Association of Sedimentologists Special Publication 27, p. 61-84.

Mora, C.I., Driese, S.G., and Colarusso, L.A., 1996, Middle to late Paleozoic atmospheric CO_2 levels from soil carbonate and organic matter: Science, v. 271, p. 1105-1107.

Murphy, E.M., and Schramke, J.A., 1998, Estimation of microbial respiration rates in ground water by geochemical modeling constrained with stable isotopes: Geochimica et Cosmochimica Acta, v. 62, p. 3395-3406.

Mutti, M., 1994, Association of tepees and paleokarst in the Ladinian Calcare-Rosso (southern Alps, Italy): Sedimentology, v. 41, p. 621-641.

Parkes, R.J., Cragg, B.A., Bale, S.J., Getliff, J.M., Goodman, K., Rochelle, P.A., Fry, J.C., Weightman, A.J., and Harvey, S.M., 1994, Deep bacterial biosphere in Pacific Ocean sediments: Nature, v. 371, p. 410-413.

Parkhurst, D.L., and Appelo, C.A.J., 1999, User's guide to PHREEQC (Version 2)— a computer program for speciation, batch-reaction, one dimensional transport, and inverse geochemical calculations: Water-Resources Investigations Report 99-4259, United States Geological Survey, 326 p.

Patchen, D.G., Avary, K.L., and Erwin, R.B., 1985, Correlation of stratigraphic units in North America - Southern Appalachian Region Chart #160: American Association of Petroleum Geologists.

Popp, B.N., Takigiku, R., Hayes, J.M., Louda, J.W., and Baker, E.W., 1986, Brachiopods as indicators of original isotopic compositions in some Paleozoic limestones: Geological Society of America Bulletin, v. 97, p. 1262-1269.

Romanek, C.S., Grossman, E.L., and Morse, J.W., 1992, Carbon isotopic fractionation in synthetic aragonite and calcite; effects of temperature and precipitation rate: Geochimica et Cosmochimica Acta, v. 56, p. 419-430.

Royes et al

Sando, W.J., 1988, Madison Limestone (Mississippian) paleokarst: a geologic synthesis, *in* Choquette, P.W., and James, N.P., eds., Paleokarst: New York, Springer-Verlag, p. 256-277.

Scotese, C.R., and Golonka, J., 1992, Paleogeographic Atlas: Arlington, Paleomap Project, University of Texas, Arlington.

Tobin, K.J., Walker, K.R., Srinivasan, K., Steinhauff, D.M., 1996, Suboxic to anoxic diagenesis of platform-marginal ooids and bladed-to-fibrous calcite from the Middle Ordovician Ottosee Formation (east Tennessee): Geological Society of America Bulletin, v. 108, p. 155-167.

Vepraskas, M.J., 1994, Redoximorphic features for identifying aquic conditions: North Carolina Agricultural Research Service, Technical Bulletin 301, 33 p.

Veizer, J., 1983, Trace elements and isotopes in sedimentary carbonates, *in* Reeder, R.J., ed., Carbonates: Mineralogy and Chemistry, Mineralogical Society of America Reviews in Mineralogy, Volume 11, p. 265-300.

Vepraskas, M.J., and Wilding, L.P., 1983, Aquic moisture regimes in soils with and without low chroma colors: Soil Science Society of America Journal, v. 47, p. 280-285.

Vepraskas, M.J., and Guertal, W.R., 1992, Morphological imdicators of soil wetness, *in* Kimble, J.M., ed., Proceedings of the Eighth International Soil Correlation Meeting: Characterization, Classification, and Utilization of Wet Soils: USDA Soil Conversation Service, Lincoln, Nebraska, p. 307-312.

Walker, K. R., Jernigan, D. G., and Weber, L. J., 1990, Petrographic criteria for the recognition of marine, syntaxial overgrowths and their distribution in geologic time: Carbonates and Evaporites, v. 5, p. 141-152.

Wilding, L.P., and Tessier, D., 1988, Genesis of Vertisols: shrink-swell phenomena, *in* Wilding, L.P. and Puentes, R. (Eds.), Vertisols: their distribution, properties, classification and management: Texas A & M University Printing Center, College Station, p. 55-81.

Wilkinson, B.H., 1979, Biomineralization, paleoceanography, and the evolution of calcareous marine organisms: Geology, v. 7, p. 524-527.

Wilson, M.A., and Palmer, T.J., 1992, Hardground and hardground faunas: University of Wales, Aberystwyth, Institute of Earth Studies Publication 9, 131 p.

Wright, V.P., 1982, The recognition and interpretation of paleokarsts: two examples from the Lower Carboniferous of South Wales: Journal of Sedimentary Petrology, v. 52, p. 83-94.

TABLE 1 - Summary of minor element data for diagenetic constituents in limestone deposits of upper Pennington Formation.

Constituent Type	Mean Mg (ppm)	Mean Ca (wt%)	Mean Mn (ppm)	Mean Fe (ppm)	n
DNF Cement (Leatherwood Ford)	2800 to 5700	-	BADL* to 600	200 to 800	8
DNF Cement (McMinnville)	500 to 2400	-	BADL to 500	BADL to 1300	26
DNF Cement (Monterey)	BADL to 900	-	300 to 700	200 to 1200	3
BL Cement (Leatherwood Ford)	400 to 3700	-	BADL to 7100	BADL to 1200	24
BL Cement (McMinnville)	BADL to 1100	-	BADL to 3500	BADL to1200	61
DF Cement (All Localities)	500 to 2800	-	BADL to 3700	1300 to 11200	139
Early, non-luminescent siderite rhomb core	8000 to 22000	3.1 to 4.8	5000 to 22600	-	6
Medial, bright luminescent calcite overgrowth	2000 to 5100	-	9100 to 11500	20500 to 79500	2
Late, nonluminescent siderite overgrowth	7500 to 31200	3.6 to 3.9	3800 to 18100	-	5
Late, very bright luminescent, fracture-filling calcite cement	BADL to 600		2500 to 3900	2500 to 4100	2
Echinoderms (Leatherwood; at paleokarst surface)	400 to 2000	-	BADL to 1600	300 to 4600	25
Echinoderms (Leatherwood; 40 cm below paleokarst)	600 to 1900	-	BADL to 300	BADL to 1000	14
Echinoderms (Leatherwood; 400 cm below paleokarst)	1500 to 2800	-	BADL to 200	BADL to 1700	18

* BADL = Below Analytical Detection Limit

TABLE 2 – Modeled meteoric water compositions.

Modeled Fluid	**Step #1 DIC** (ppm of C)	**Mg** (ppm)	**Ca** (ppm)	**Mg/Ca Ratio**	**Fe** (ppm)	**Step #3 DIC ($C_{f,o}$)** (ppm of C)	**pH**
River Water A	12.5	3.8	14.6	0.4	0.25	16.2	7.2
River Water B	12.5	3.8	14.6	0.4	1.0	16.2	7.3
River Water C	12.5	3.8	14.6	0.4	4.0	16.2	8.0
1A	3.1	0.6	4.2	0.25	1.0	7.0	6.7
1B	3.1	1.0	3.5	0.5	1.0	7.0	6.7
1C	3.1	1.6	2.6	1.0	1.0	7.0	6.7
2A	6.2	1.2	8.2	0.25	1.0	10.1	7.0
2B	6.2	2.1	7.0	0.5	1.0	10.1	7.0
2C	6.2	3.1	5.2	1.0	1.0	10.1	7.0
3A	12.5	2.5	16.7	0.25	1.0	16.2	7.3
3B	12.5	4.2	13.9	0.5	1.0	16.2	7.3
3C	12.5	6.2	10.4	1.0	1.0	16.2	7.3
4A	25.0	4.9	33.4	0.25	1.0	28.3	7.6
4B	25.0	8.2	27.8	0.5	1.0	28.3	7.6
4C	25.0	12.3	20.9	1.0	1.0	28.4	7.6

TABLE 3 - Parameters used in fluid-rock calculations for $\delta^{13}C$ and $\delta^{18}O$ isotope systems.

	Carbon ($\delta^{13}C$)	Oxygen ($\delta^{18}O$)
($\alpha_{calcite\text{-}H}$) @ 25 °C	1.001	1.0285
($C^{o}_{f,o}$) (in ppm)	See Table 2; Step #3 DIC	890000
($C^{o}_{calcite,o}$) and ($C^{o}_{calcite}$) (in ppm)	120000	480000
(C^{o}_{o}) (in ppm)	Varies based on Step #3 DIC; ($C^{o}_{f,o}$)	536000
($\delta_{f,o}$)	-11.0 ‰ PDB	-3.6 ‰ SMOW
Initial ($\delta_{calcite,o}$)	4.0 ‰ PDB	-2.0 ‰ PDB

TABLE 4 - Parameters used in fluid-rock calculations for Mg and Fe systems.

	Mg	**Fe**
($C_{calcite,o}$)	12 wt.%	2 ppm
(C_f) (in ppm)	See Table 2; Mg (ppm)	See Table 2; Fe (ppm)
($C_{calcite,e}$)	1200 ppm	_____
Fe (K_D)	_____	1.9
Ca (C_f) (in ppm)	_____	See Table 2; Ca (ppm)

TABLE 5 – Calculated Saturation Indexes for Selected Minerals.

Modeled Fluid	Calcite SI	Siderite SI
River Water A	-1.2	-0.7
River Water B	-1.1	0
River Water C	-0.3	1.3
1A	-2.7	-1.1
1B	-2.8	-1.1
1C	-2.9	-1.1
2A	-1.9	-0.6
2B	-2.0	-0.6
2C	-2.1	-0.6
3A	-1.0	0
3B	-1.1	0
3C	-1.2	0
4A	-0.1	0.6
4B	-0.2	0.6
4C	-0.3	0.6

FIGURE CAPTIONS

Figure 1 - Claystone paleosol overlying paleokarst surface at Leatherwood Ford locality. **(A)** Outcrop photograph showing prominent pedogenic slickensides (arcuate features) and angular blocky ped structures. Note that drab coloration dominates in upper part of paleosol, whereas darker coloration characterizes lower part. Scale card is 15 cm. **(B)** Thin-section photograph showing rhombohedral ped with redox enrichment of Mn and Fe on ped face and redox depletion (*sensu* Vepraskas 1992) in interpedal area. Scale in centimeters. **(C)** Thin-section photomicrograph showing redox depletion and redox enrichments around ped margin shown in sample **(B)**. Plane-polarized light. **(D)** Thin-section photomicrograph showing hematite spherules in paleosol matrix. Note Fe depletion "halos" around spherules. Plane-polarized light.

Figure 2 - Vertic claystone paleosol developed on limestone saprolite, primarily from clay sediment parent material, at Leatherwood Ford locality. **(A)** Stratigraphic log showing color, horizonation, and soil structures observed in outcrop sections. **(B)** Mass-balance geochemistry of selected elements from vertic claystone paleosol at Leatherwood Ford locality, calculated assuming Ti immobility, showing net gains or losses of elements relative to model parent material at base of paleosol. To convert to percentages, multiply values times 100. Net gains are observed for Na (■), Ca (◆), and K (▲). Significant losses of Mn (★) and Fe (✖) are observed; whereas, Si (●) exhibits limited change.

Figure 3 - Photomicrographs of diagenetic features from upper Pennington Formation limestones at McMinnville locality. **(A)** Large calcite spar cement-filled shelter and intergranular pores in echinoderm-bioclast grainstone (plane light). **(B)** Same field of view as in **(A)**, but under cathodoluminescence (CL) conditions. Note echinoderm grain (E), dully luminescent, nonferroan calcite cement (DNF) grown syntaxially on echinoderm grain (arrow), banded bright-dark luminescent, non-ferroan calcite spar cement (BL), and final pore-occluding, dull luminescent,

ferroan calcite spar cement (DF). Dark areas at upper right and bottom left of photo were not excited by the electron beam. **(C)** Subset of field of view in **(B)**, under CL conditions. Note presence of dull luminescent, non-ferroan calcite spar cement (DNF) grown syntaxially on echinoderm host grain (E). **(D)** Subset of field of view in **(B)**, under CL conditions. Note very small amount of bladed DNF cement nucleated on pore wall, followed by complexly zoned BL cement, and final pore-occluding DF cement.

Figure 4 - **(A, B)** Paired transmitted light/CL photomicrographs of zoned siderite that crosscuts all DF cement. Siderite exhibits distinct zoning with nonluminescent core, thin bright luminescent band, and nonluminescent rim. **(C, D)** Paired transmitted light/CL photomicrographs of large echinoderm grain. In CL skeletal calcite is dull luminescent with patches of bright luminescent calcite. Micropores are occluded by calcite cement that is nonluminescent.

Figure 5 - Cross-plot of Mg versus Fe for **(A)** BL cement and **(B)** echinoderm grains from the Leatherwood Ford locality. Echinoderms in sample immediately below the paleokarst surface have the highest Mn and Fe values (circles) compared with echinoderms 40 cm (diamonds) and 400 cm (squares) below the paleokarst surface. Note: analyses below detection limits within the gray fields do not represent real numbers, but are shown in order to better indicate the relative number of sample points.

Figure 6 - $\delta^{13}C$ versus $\delta^{18}O$ cross-plot for echinoderm grains, which define a meteoric line as indicated with a characteristic inverted "J" pattern of isotope covariation (Lohmann 1988). Star reflects likely Carboniferous marine value after Meyers and Lohmann (1985) and Popp et al. (1986). Curved line is derived from iterative fluid-rock modeling of $\delta^{13}C$ and $\delta^{18}O$ (Banner and Hanson 1990) and N reflects cumulative fluid-rock ratio (see text; calculated based on River Water B solution composition). Inset shows depth-dependent variation of $\delta^{13}C$ values from

McMinnville echinoderms with depth of samples below the paleokarst surface with analyses as indicated (0 cm = ▼; 5 cm = ●; 10 cm = +; 25 cm = ■; 125 cm = ×; 400 cm = ✔).

Figure 7 - Curved lines are derived from iterative fluid-rock modeling of Mg and Fe (Banner and Hanson 1990) and N reflects cumulative fluid-rock ratio using different solution compositions (see text; red line – River Water A; green line – River Water B; blue line – River Water C). Observed echinoderms Mg and Fe values are also plotted (sample immediately below the paleokarst surface (solid field), 40 cm below paleokarst surface (open field) and 400 cm below paleokarst surface (dashed field). Note: analyses below detection limits within the gray fields do not represent real numbers, but are shown in order to better indicate the relative number of sample points.

Figure 8 - Curved lines are derived from iterative fluid-rock modeling of Mg and Fe (Banner and Hanson 1990) and N reflects cumulative fluid-rock ratio using different solution compositions (Figure 8A - Series 1; Figure 8B – Series 2; red line – Mg/Ca ratio = 1; green line – Mg/Ca ratio = 0.5; blue line – Mg/Ca ratio = 0.25). Observed echinoderms Mg and Fe values are also plotted (sample immediately below the paleokarst surface (solid field), 40 cm below paleokarst surface (open field) and 400 cm below paleokarst surface (dashed field). Note: analyses below detection limits within the gray fields do not represent real numbers, but are shown in order to better indicate the relative number of sample points.

Figure 9 - Curved lines are derived from iterative fluid-rock modeling of Mg and Fe (Banner and Hanson 1990) and N reflects cumulative fluid-rock ratio using different solution compositions (Figure 9A - Series 3; Figure 9B – Series 4; red line – Mg/Ca ratio = 1; green line – Mg/Ca ratio = 0.5; blue line – Mg/Ca ratio = 0.25). Observed echinoderms Mg and Fe values are also plotted (sample immediately below the paleokarst surface (solid field), 40 cm below paleokarst surface (open field) and 400 cm below paleokarst surface (dashed field). Note: analyses below detection

limits within the gray fields do not represent real numbers, but are shown in order to better indicate the relative number of sample points.

Figure 10 - Generalized diagram depicting sub-aerial exposure and formation of paleokarst at the Mississippian-Pennsylvanian boundary. See text for detailed discussion of this diagram.

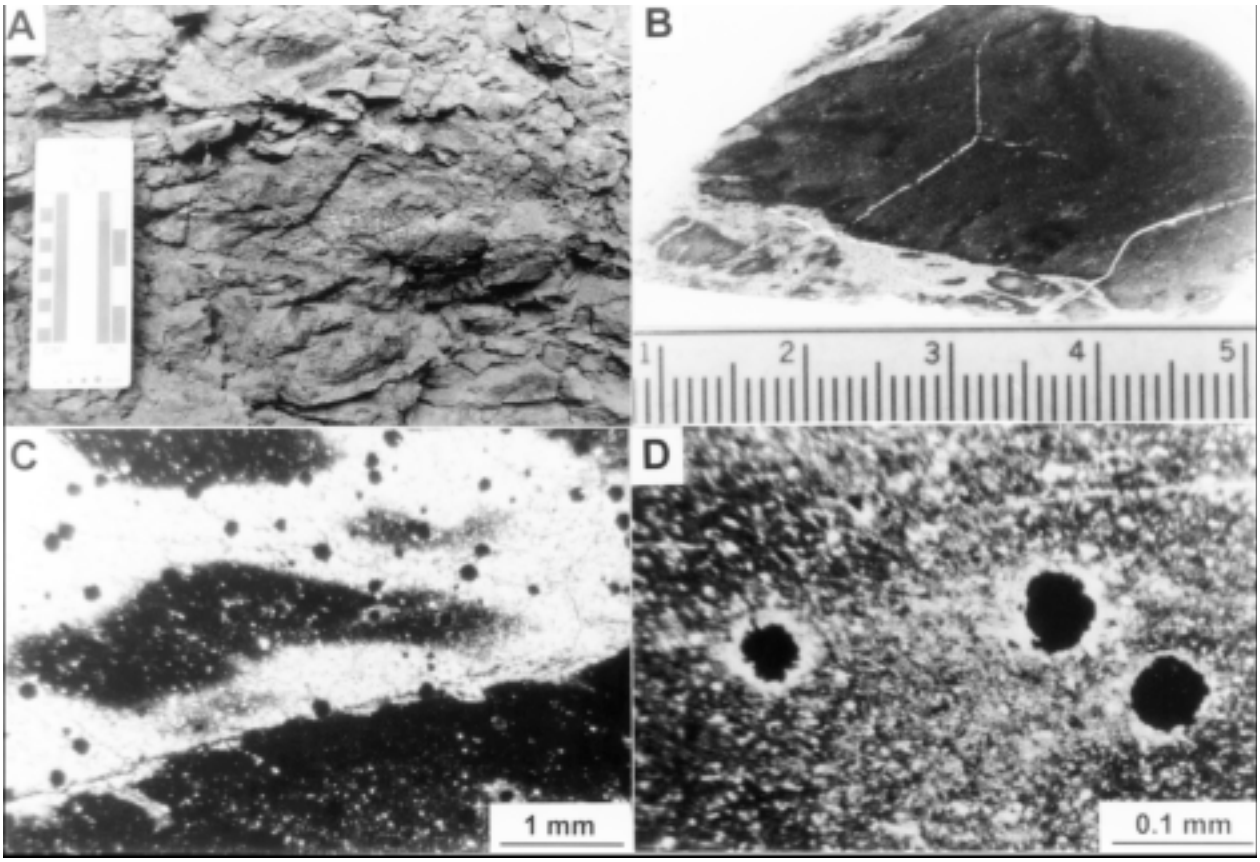

Figure 1

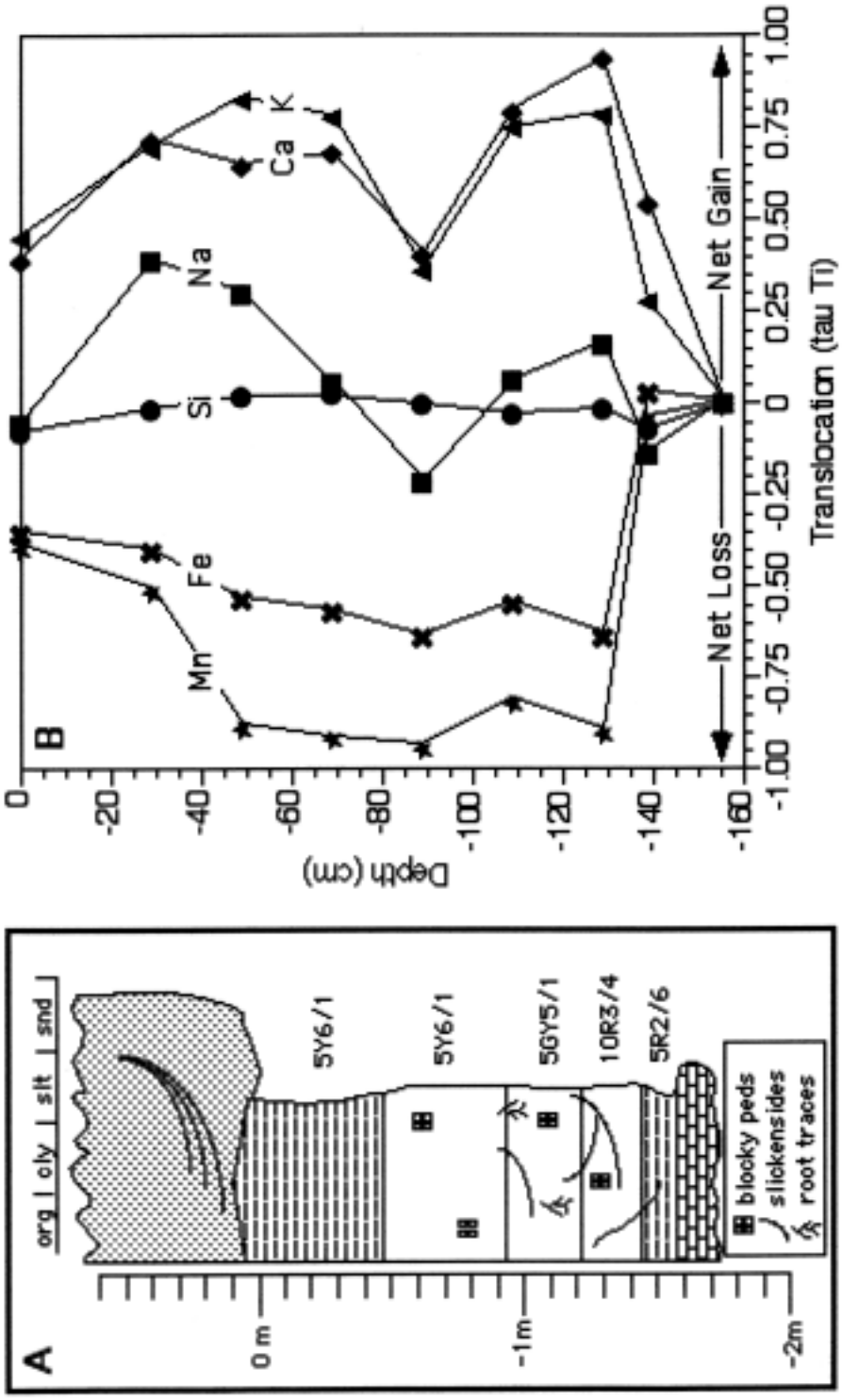
A
org | oly | slt | snd
5Y6/1
5Y6/1
5GY5/1
10R3/4
5R2/6
blocky peds
slickensides
root traces
0 m
-1m
-2m
B
Mn
Fe
Si
Na
Ca
K
Depth (cm)
0
-20
-40
-60
-80
-100
-120
-140
-160
Net Loss
Net Gain
-1.00
-0.75
-0.50
-0.25
0
0.25
0.50
0.75
1.00
Translocation (tau Ti)

Figure 2

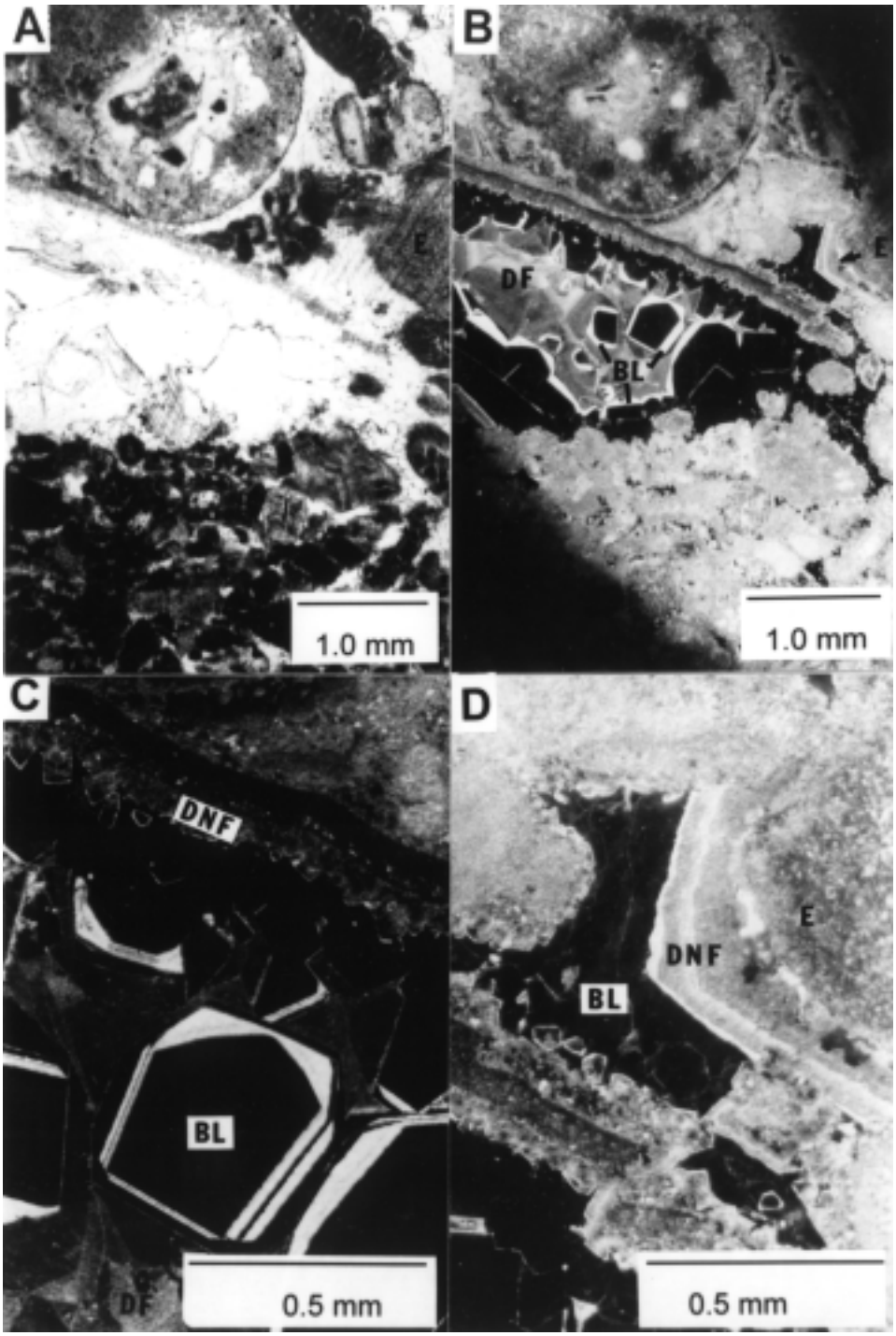

Figure 3

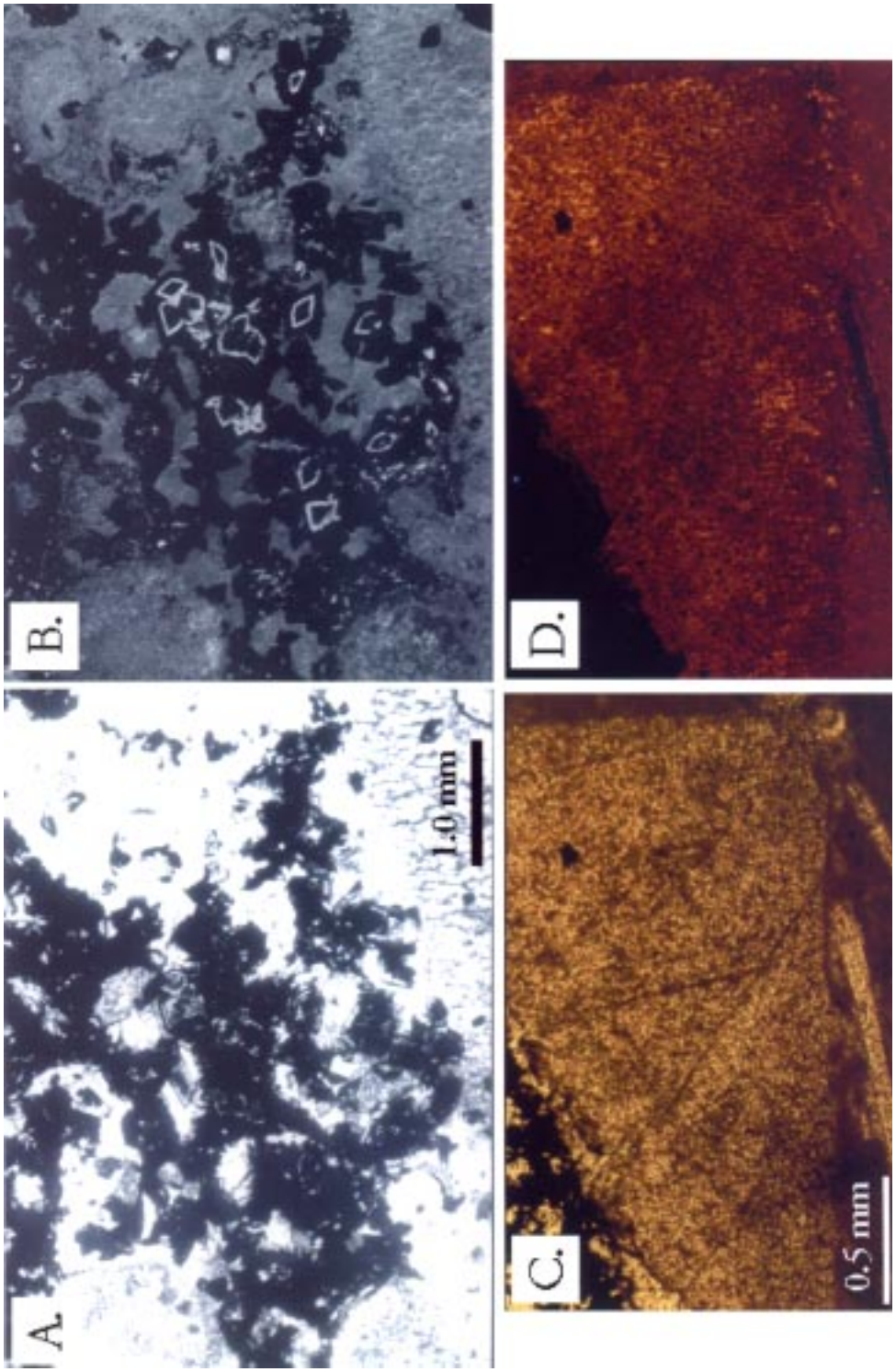

Figure 4

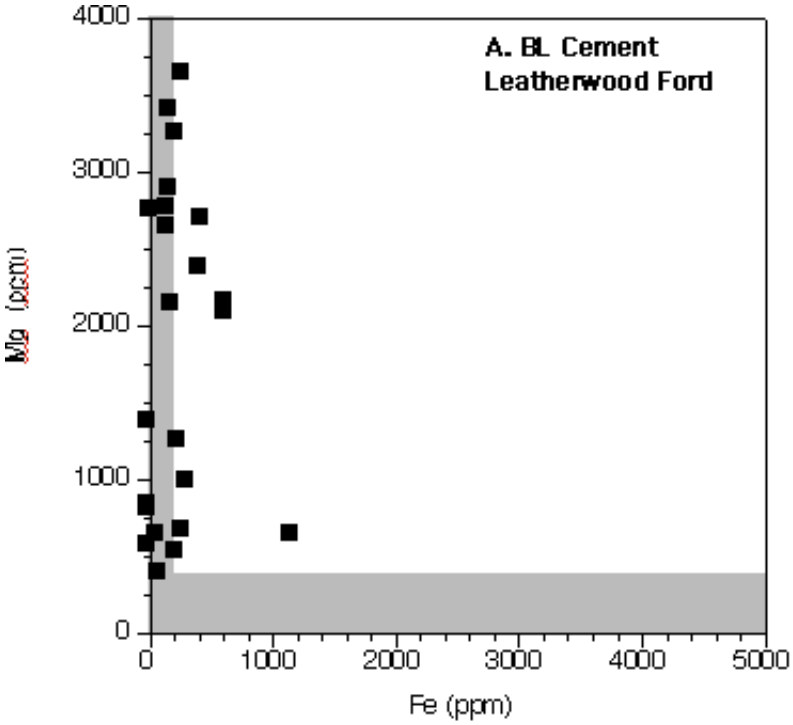
A. BL Cement
Leatherwood Ford
Mg (ppm)
Fe (ppm)
0
1000
2000
3000
4000
5000

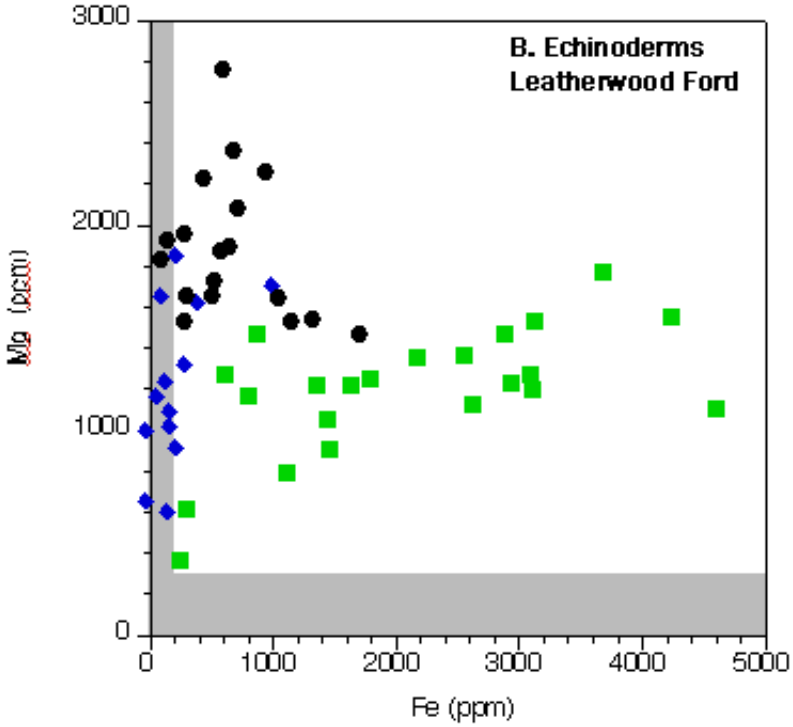
B. Echinoderms
Leatherwood Ford
Mg (ppm)
Fe (ppm)
0
1000
2000
3000
4000
5000

Figure 5

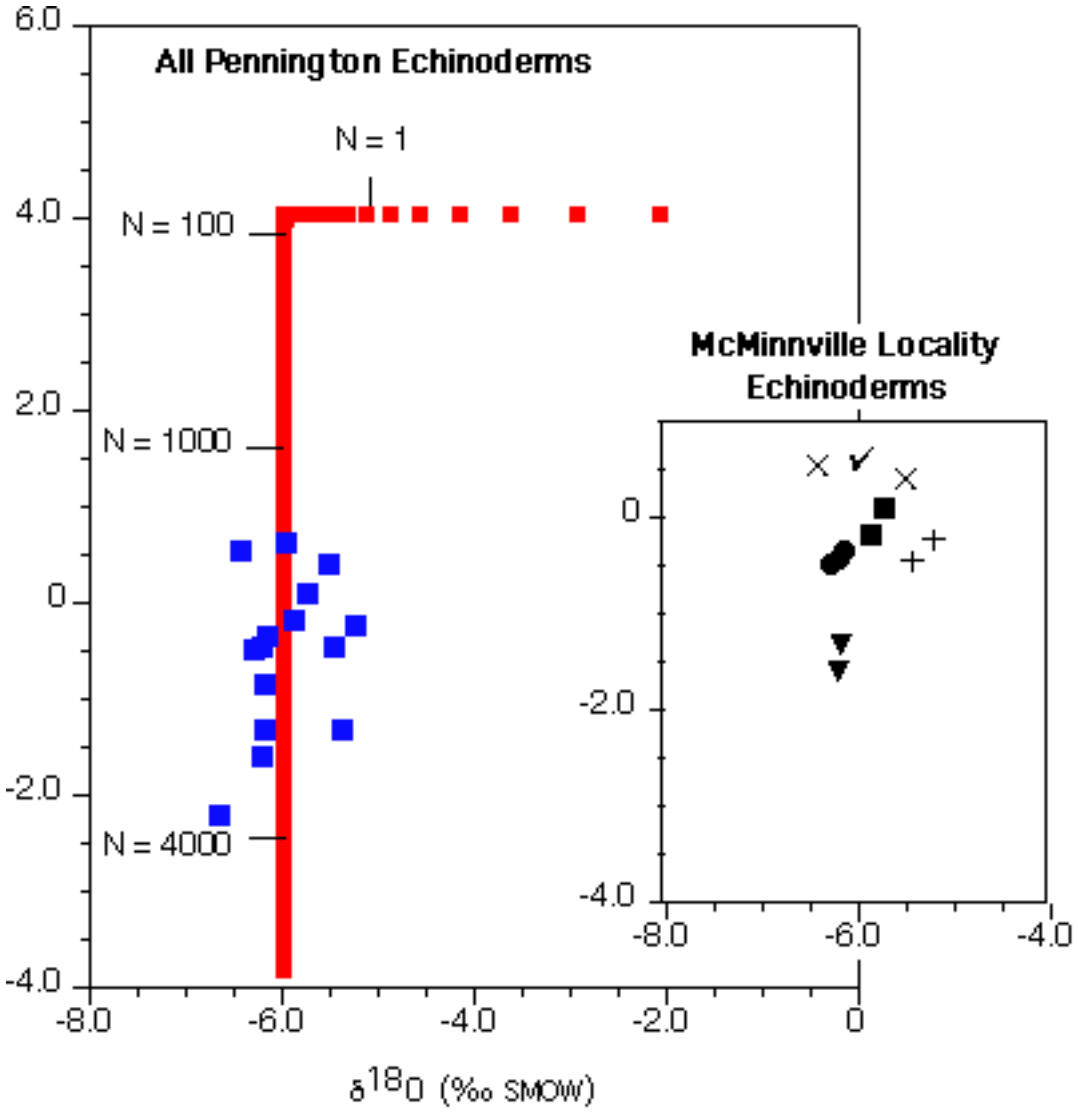
All Pennington Echinoderms
N = 1
N = 100
N = 1000
N = 4000
McMinnville Locality
Echinoderms
6.0
4.0
2.0
0
-2.0
-4.0
-8.0
-6.0
-4.0
-2.0
0
δ18O (‰ SMOW)

Figure 6

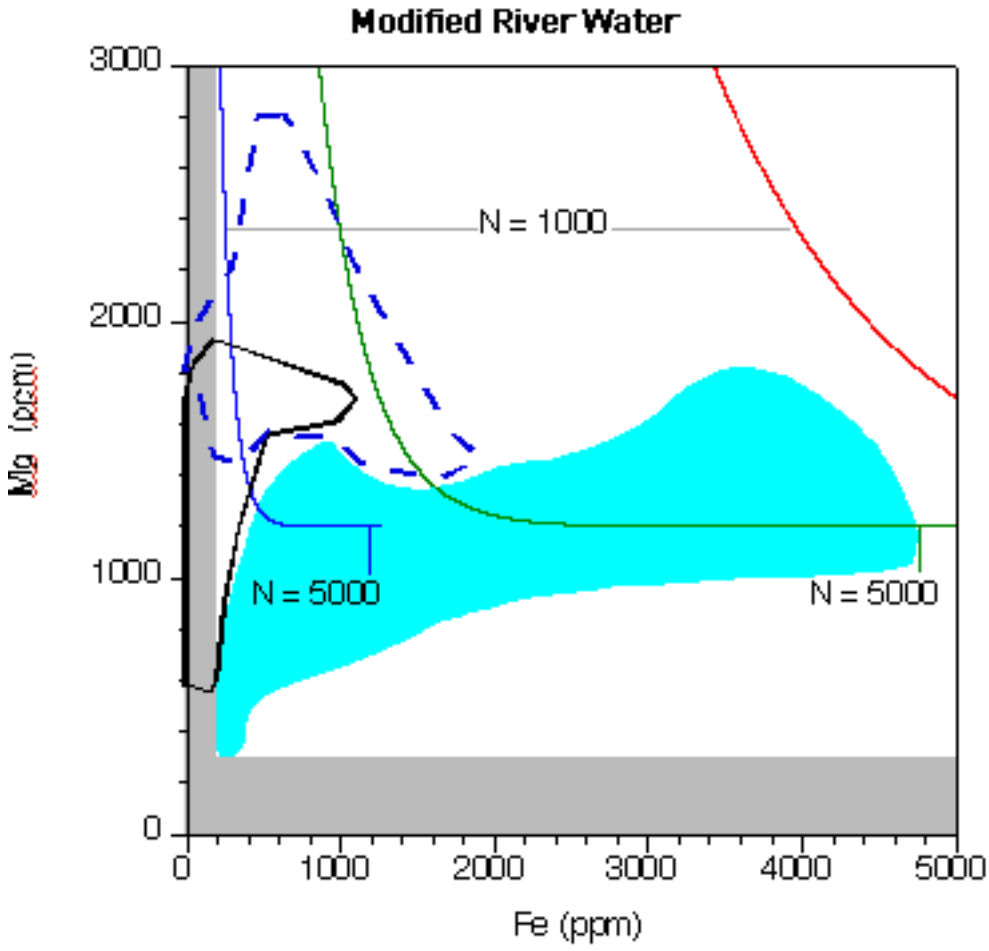
Modified River Water
3000
2000
1000
0
Mg (ppm)
N = 1000
N = 5000
N = 5000
0
1000
2000
3000
4000
5000
Fe (ppm)

Figure 7

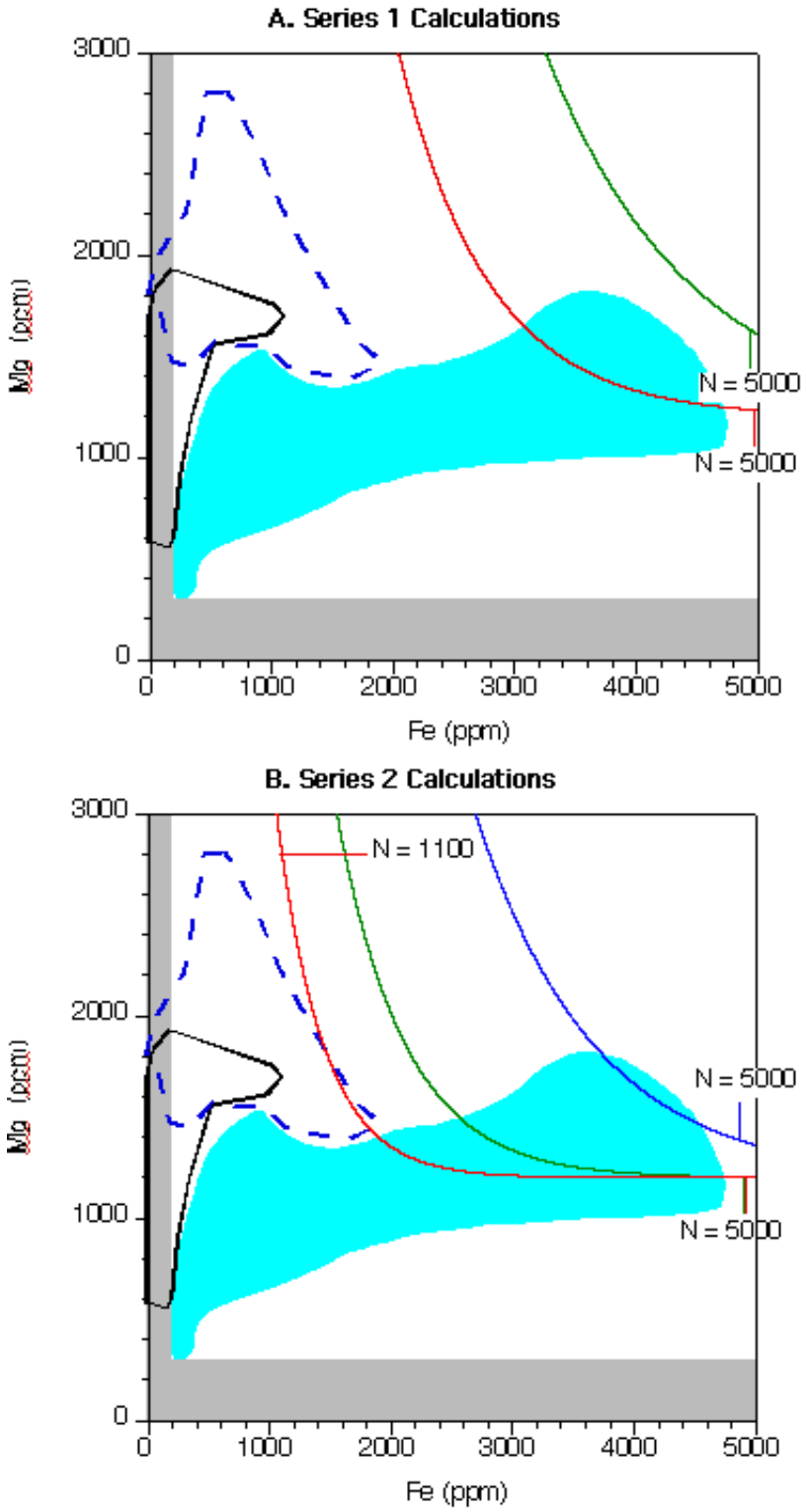
A. Series 1 Calculations
3000
2000
1000
0
Mg (ppm)
N = 5000
N = 5000
0
1000
2000
3000
4000
5000
Fe (ppm)
B. Series 2 Calculations
3000
2000
1000
0
Mg (ppm)
N = 1100
N = 5000
N = 5000
0
1000
2000
3000
4000
5000
Fe (ppm)

Figure 8

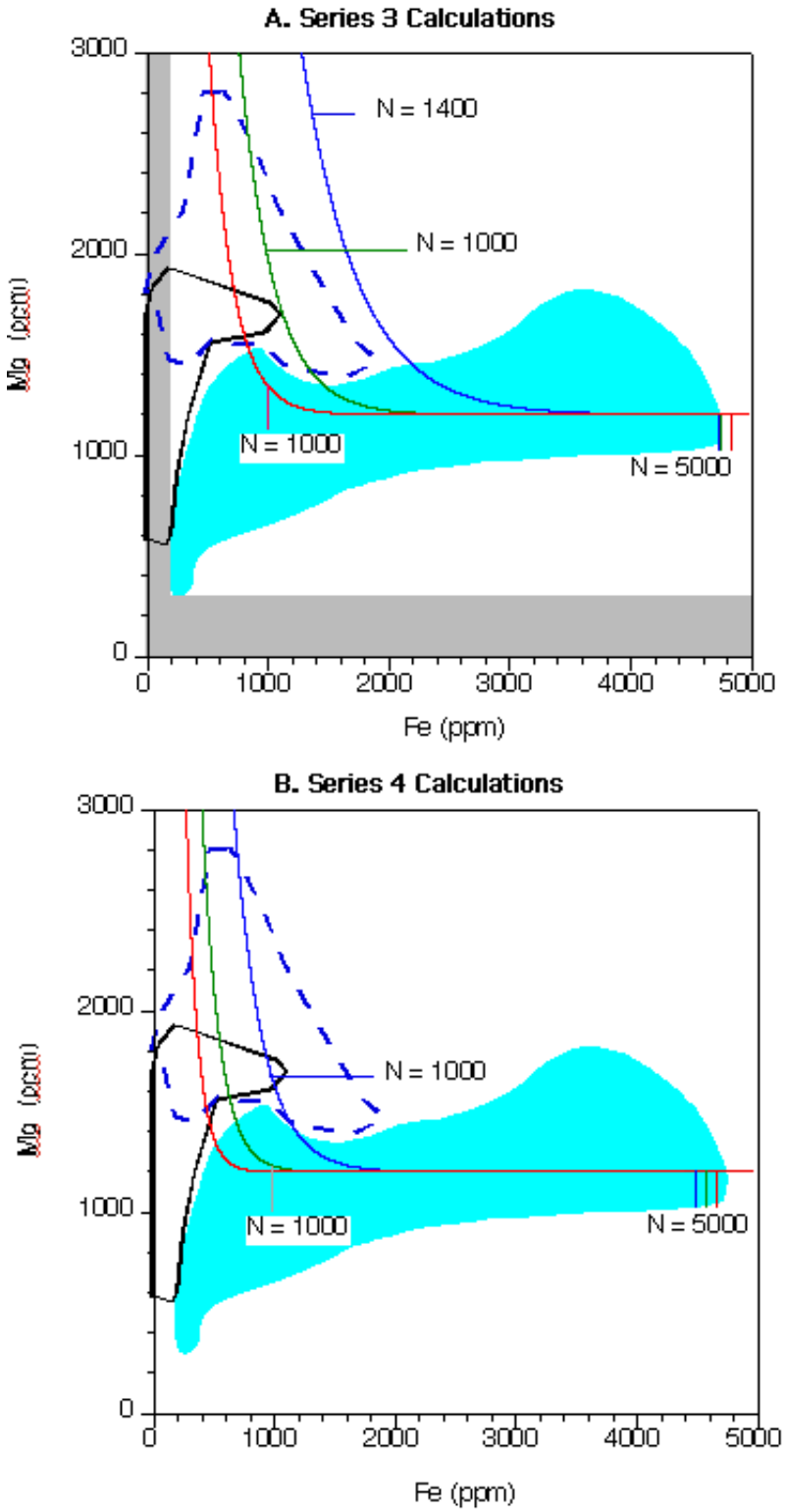
A. Series 3 Calculations
3000
2000
1000
0
Mg (ppm)
N = 1400
N = 1000
N = 1000
N = 5000
0
1000
2000
3000
4000
5000
Fe (ppm)
B. Series 4 Calculations
3000
2000
1000
0
Mg (ppm)
N = 1000
N = 1000
N = 5000
0
1000
2000
3000
4000
5000
Fe (ppm)

Figure 9

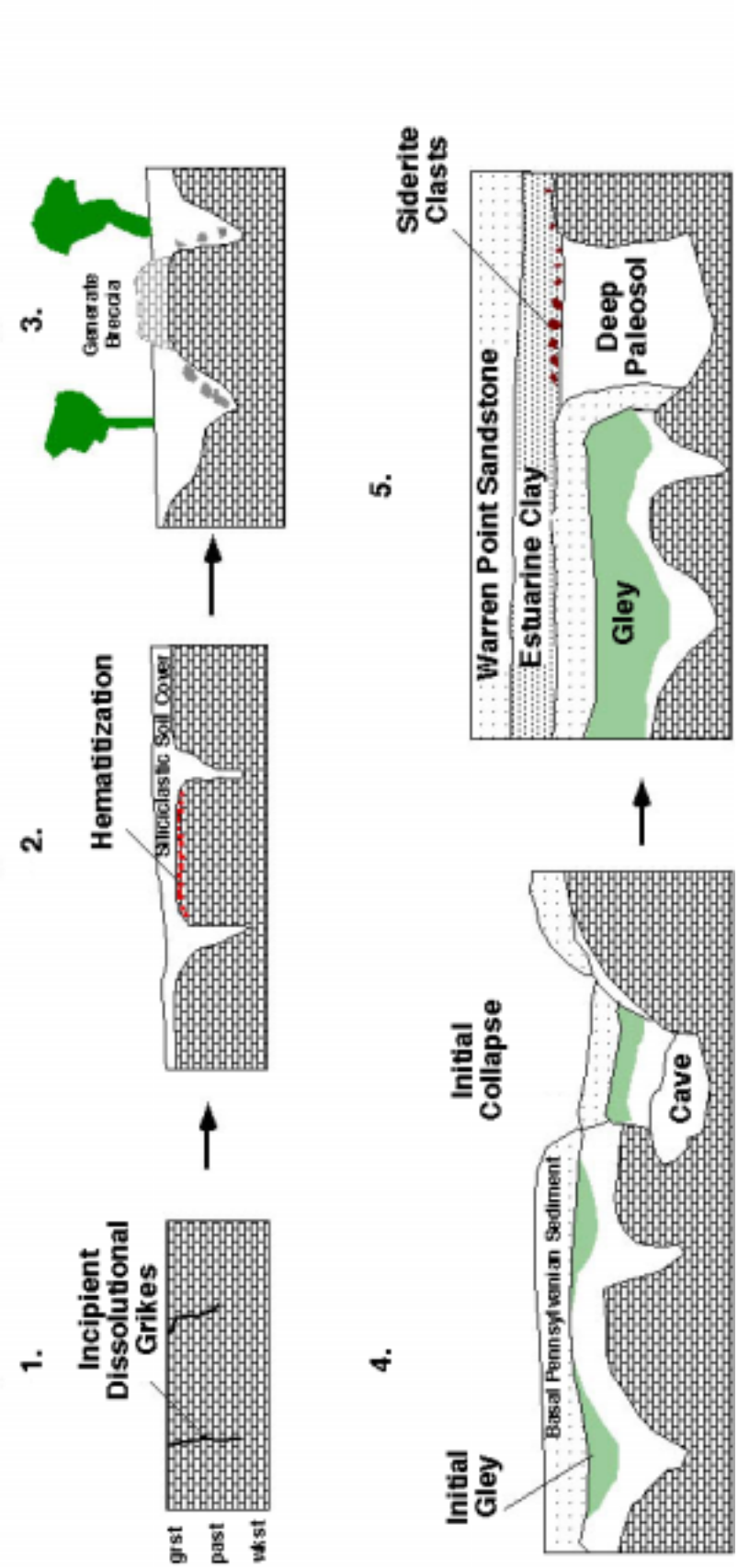
1.
Incipient Dissolutional Grikes
2.
Hematitization
Siliciclastic Soil Cover
3.
Cenozoic Breccia
4.
Initial Collapse
Cave
Basal Pennsylvanian Sediment
Initial Gley
5.
Siderite Clasts
Warren Point Sandstone
Estuarine Clay
Gley
Deep Paleosol

Figure 10